



# Retrieval of Aerosol Properties from Direct Solar Irradiance Measurements with High Temporal Resolution and Spectral Range

Angelos Karanikolas<sup>1,2\*</sup>, Benjamin Torres<sup>4</sup>, Masahiro Momoi<sup>3</sup>, Marcos Herreras Giralda<sup>3</sup>, Natalia Kouremeti<sup>1</sup>, Julian Gröbner<sup>1</sup>, Lionel Doppler<sup>5</sup> and Stelios Kazadzis<sup>1</sup>

5 <sup>1</sup> World Optical Depth Research and Calibration Centre (WORCC), Physikalisch-Meteorologisches Observatorium Davos/World Radiation Center (PMOD/WRC), Davos Dorf, 7260, Switzerland

<sup>2</sup> Institute for Particle Physics and Astrophysics, ETH Zurich, Zurich, 8093, Switzerland

<sup>3</sup> GRASP SAS, Lille, 59800, France

<sup>4</sup>Laboratoire d'Optique Atmosphérique (LOA), University of Lille, Lille, 59000, France

10 <sup>5</sup>Deutscher Wetterdienst (DWD), Meteorologisches Observatorium Lindenberg (MOL-RAO), Lindenberg (Tauche), 15848, Germany

*Correspondence to:* Angelos Karanikolas (angelos.karanikolas@pmodwrc.ch)

**Abstract.** Several sun photometer networks worldwide include instruments for aerosol optical depth (AOD) observations, such as Global Atmospheric Watch-Precision Filter Radiometer (GAW-PFR) and Aerosol Robotic Network (AERONET). AERONET provides additional aerosol properties such as the detailed volume size distribution and the single scattering albedo through inversion modelling of sky radiance measurements. However, the data availability for such properties is limited due to the limited number of daily almucantar sky radiance scans and cloudiness. AOD measurements are significantly more frequent as they can be even every minute and are affected only by clouds being too close or covering the solar disk. The Generalized Retrieval of Atmosphere and Surface Properties (GRASP) is a flexible inversion model to retrieve aerosol properties from various observations. One of its capabilities is the retrieval of the volume concentration, the volume median radius and geometric standard deviation for each aerosol size distribution mode and the separation of AOD to each mode using only spectral AOD as an input parameter. Such properties are important for various applications, as the size of aerosols affects their interaction with solar radiation, clouds and radiative forcing modelling. Size also shows significant differences depending on the aerosol type such as dust or biomass burning. In this study, we selected four common stations of GAW-PFR and AERONET and used GRASP to retrieve the bimodal size distribution parameters from AOD measured by GAW-PFR instruments (PFRs). We assessed the homogeneity with the AERONET output parameters and investigated the effect of the spectral range and on such retrievals. We also assessed the performance for certain dust and biomass burning cases. Our results showed good agreement between PFR AOD-based and AERONET sky radiance inversions for AOD modal separation and volume concentrations. Significant improvement of the PFR-AERONET intercomparison was also possible for the fine mode volume and effective radius when restricting the datasets to AOD at 500 nm > 0.1 and Angström Exponent (AE) > 1. Also, the results showed consistency with previous study regarding the validation of such retrievals using AERONET AOD. Focusing on conditions with high proportion of dust particles, we found consistent results with the general cases.



Using AOD with a larger spectral range (from BTS spectroradiometer), we found that the wavelength selection may affect the  
35 results and that using longer wavelengths can increase the sensitivity of coarse mode volume median radius to AOD and  
improve the correlation of the GRASP BTS AOD-based and AERONET datasets. However, the available data were limited,  
so it is not clear under what conditions the inclusion of such wavelengths will result in more accurate retrievals.

Finally, we were able to reproduce with GRASP the aerosol size characteristics of unusual biomass burning cases from the  
Canadian wildfires during 2023, but the results showed systematically increased fine mode radius and concentration compared  
40 to the AERONET output.

## 1 Introduction

Atmospheric aerosols are critical in atmospheric science and environmental studies. By scattering and absorbing solar  
radiation, they influence the amount of radiation that reaches Earth's surface, thereby impacting ecosystems' exposure to  
45 biologically active radiation (Horneck, 1995; Bais et al., 2018; Barnes et al., 2019), the efficiency of solar energy systems  
(Myers, 2005; Hou et al., 2022; Papachristopoulou et al., 2024), and the planet's energy balance (Hodnebrog et al., 2024). Over  
recent decades, aerosols have significantly contributed to variations in surface solar irradiance (Wild, 2012; Wild et al., 2021;  
Correa et al., 2024). They play a vital role in cloud formation and can modify cloud characteristics (Winkler and Wagner,  
2022; Maloney et al., 2022). The influence of aerosols on solar radiation serves as a key driver for climate and weather patterns  
50 (IPCC, 2023). Improved aerosol monitoring is therefore an important factor to consider for reducing the uncertainty in the  
attribution of radiative forcing (Rosenfeld et al., 2014; IPCC, 2023) and improving weather forecasts (Glotfelty et al., 2019;  
Huang and Ding, 2021). Additionally, aerosols are significant air pollutants affecting human health, particularly those with  
radii under 2.5  $\mu\text{m}$ , which are major contributors to premature mortality, causing millions of deaths annually (Xiang et al.,  
2021; Yu et al., 2024).

55 Aerosol optical depth (AOD) is a key parameter in studying Earth's energy budget concerning aerosols (WMO, 2003). AOD  
quantifies the total extinction of solar radiation as it passes through the atmosphere due to aerosols. It is mathematically  
represented through the Beer-Lambert-Bouguer law:

$$I = I_0 e^{-m\tau} \quad (1)$$

where  $I$  is the solar irradiance at the surface,  $I_0$  is the irradiance at the top of the atmosphere,  $m$  represents the air mass  
60 coefficient and  $\tau$  the atmospheric optical depth. The optical depth is the sum of the optical depth from all atmospheric  
components, so AOD is a component of  $\tau$ .

AOD is also approximated by the Ångström law:

$$\tau_a = \beta \lambda^{-\alpha} \quad (2)$$



65 where  $\beta$  denotes the turbidity coefficient,  $\lambda$  is the wavelength, and  $\alpha$  represents the Ångström exponent (AE). The turbidity coefficient  $\beta$  correlates with aerosol concentration, while the wavelength dependence of  $\tau$ , indicated by  $\alpha$ , relates to aerosol size.

AOD measurements are conducted using instruments that measure direct solar irradiance (DSI) under cloudless conditions at wavelengths minimally affected by gas absorption, reducing uncertainties in optical depth corrections for trace gases. Sun photometers are the primary tools for AOD measurements, measuring DSI at specific wavelengths. Various sun photometer  
70 types are organized into global networks, including the Aerosol Robotic Network (AERONET) (Holben et al., 1998; Giles et al., 2019), the Global Atmosphere Watch-Precision Filter Radiometer (GAW-PFR) (Kazadzis et al., 2018b), and SKYNET (Nakajima et al., 2020). AERONET comprises over 500 stations worldwide, utilizing the CIMEL CE318-TS sun and sky photometer (CIMEL) as its standard instrument (Barreto et al., 2016). GAW-PFR consists of 14 core and 14 associated stations globally, predominantly situated in remote areas. It employs the Precision Filter Radiometer (PFR) and incorporates the WMO  
75 reference instruments (PFR-Triad) for AOD measurements (Kazadzis et al., 2018b). SKYNET is composed of various instrument types divided into sub-networks, covering approximately 100 sites, primarily in East Asia and the western Mediterranean. Its primary instrument for AOD and aerosol property measurements is the PREDE-POM sun and sky radiometer (POM) (Nakajima et al., 2020). In this study, we focus on GAW-PFR and AERONET. Several studies have displayed good homogenization between the AOD of these two networks on short-term campaigns (Mazzola et al., 2012; Kazadzis et al., 2018a; Kazadzis et al., 2023) and long-term observations (Cuevas et al., 2019; Karanikolas et al., 2022). Other  
80 instruments, such as spectroradiometers can provide AOD observations with larger spectral range and resolution, although the accuracy can be limited by strong gas absorption at certain wavelengths (Kazadzis et al., 2007; Cachorro et al., 2009; Fountoulakis et al., 2019; Gröbner et al., 2023).

Aside from AOD, there are other aerosol properties that refer to the total aerosol column, such as the aerosol size distribution  
85 (SD) and the aerosol optical properties such as refractive index or single scattering albedo (SSA). The SD describes the volume concentration of aerosols in relation to their radius and can be typically approximated as a bimodal lognormal function (Schuster et al., 2006). SD can be described by six parameters (three for each mode, fine and coarse in our case): the fine and coarse mode components of the volume concentration ( $C_{Vf}$  and  $C_{Vc}$ ), the volume median radius ( $R_{Vf}$  and  $R_{Vc}$ ) and the geometric standard deviation ( $\sigma_{Vf}$  and  $\sigma_{Vc}$ ) (Torres and Fuertes, 2021). The SD and additional aerosol properties (such as the SSA, the  
90 real (RRI) and imaginary (IRI) part of the refractive index) are typically retrieved through the inverse modelling of sky radiance observations at the almucantar geometry (Dubovik and King, 2000). The main network providing such properties is AERONET. AERONET also provides the separation of AOD into each mode, fine mode AOD ( $AOD_f$ ) and coarse mode AOD ( $AOD_c$ ) through two different methodologies. One is the inversion of sky radiance (Dubovik and King, 2000) and the other is through the spectral deconvolution algorithm (O'Neil et al., 2003).

95 The sky radiance scans are performed once per hour for solar zenith angles (SZA)  $< 54^\circ$  and at four specific angles (eight scans per day) for SZA  $\geq 54^\circ$  (Sinyuk et al., 2020), while AOD observations are typically performed with a temporal resolution in the range of 1 to 15 minutes depending on the instrument, time and location (Cuevas et al., 2019). However, there were



methodologies developed to retrieve the SD parameters using only AOD observations (King, 1978; King, 1982; Wendisch and von Hoyningen-Huene, 1994). Several newer studies include such methodologies (Schuster, 2006; Kazadzis et al., 2014; Perez-Ramirez et al., 2015; Torres et al., 2017). In Kazadzis et al., (2014), AOD is used to retrieve the total volume concentration ( $C_{VT}$ ) and the effective radius ( $R_{eff}$ ) through a linear estimation technique (Veselovskii et al., 2012). The Generalized Retrieval of Atmosphere and Surface Properties (GRASP) (Dubovik et al., 2014; Dubovik et al., 2021) is a flexible algorithm used for retrievals of aerosol properties using observations from various instruments. It also includes the capability to retrieve the six SD parameters described earlier and the  $AOD_f$  and  $AOD_c$  as derived products using only AOD observations (Torres et al., 2017). The methodology was validated for AOD from AERONET at different sites (Torres and Fuertes, 2021).

The size of aerosols plays an important role in several different processes and applications. Size affects the interaction of radiation with aerosols (Ezhova et al., 2018) by altering their scattering (Witriol and Sindoni, 1992) and absorption capabilities (Tian et al., 2023), including relative response between different wavelengths (Pandolfi et al., 2018). Size is particularly important for the computation of the aerosol asymmetry factor (Andrews et al., 2006; Ehlers and Moosmüller, 2023) as the asymmetry factor and phase function show significant sensitivity to size (Li et al., 2022). Large particles like dust show increased forward scattering (Cuevas et al., 2019; Liu et al., 2023), which affects the diffuse solar irradiance distribution and fraction (Li et al., 2023).

The size can indicate the aerosol type and under certain conditions it is a main difference between anthropogenic and natural aerosols. Natural aerosols tend to be larger and contribute more to the coarse mode aerosols, with types such as dust (Mona et al., 2014; Monteiro et al., 2018; Shao et al., 2020; Konsta et al., 2021; Barreto et al., 2022), pollen and other biogenic particles (except viruses) (Maser and Jaenicke, 1995; Mampage et al., 2022) and sea salt (Ackerman et al., 2023). However, volcanic aerosol sizes vary significantly depending on the type, so they can contribute to a larger extent in the fine mode. A volcanic eruption may either increase or decrease the aerosol size locally (Martin et al., 2008; Wrana et al., 2023). Anthropogenic aerosol emissions are mostly in the fine mode (Xia et al., 2007; Deng et al., 2022) or even with a significant contribution of ultra fine particles through combustion for industrial, heating and transport purposes (Tiwari et al., 2014; Zhang et al., 2022; Abdillah et al., 2024). Coarse mode particles are also emitted though, mostly through mechanical processes (Wu and Boor, 2021). Finally, one of the main aerosol types on Earth is the smoke from biomass burning (mostly from large wildfires), which can be either natural or anthropogenic and corresponds mostly to the fine mode (Alonso-Blanco et al., 2014; Shi et al., 2019; Masoom et al., 2023). As aerosols are crucial for cloud nucleation, their size also plays an important role in water droplet and ice crystal formation hence in cloud cover and properties as well (Svenningsson et al., 1997; Levin et al., 2003; Hernández Pardo et al., 2019). This can also lead to implications in modelling cloud properties, such as droplet number concentration and cloud albedo, depending on the aerosol size distribution used (Kodros and Pierce, 2017) and the radiative forcing attribution to aerosols and clouds (Virtanen et al., 2025). Reduced cloud coverage also seems to be the main reason for the unusually high global temperature in 2023 that was not solely explained by anthropogenic global warming due to greenhouse gas emissions and the El Niño-Southern Oscillation phase (Goessling et al., 2024), where the role of aerosols remains yet unclear. The size of aerosols is also one of the main parameters affecting the transport range of aerosols and the deposition rate (Nicolae et al.,



2019; Rodríguez-Arias et al., 2023). As larger particles tend to be more massive, their residence time in the atmosphere is decreased due to gravity. Aerosols are also responsible for various health effects and their size is one of the key parameters to describe those effects. Depending on the size, they can infiltrate and affect different parts of the body (Kodros et al., 2018), with smaller aerosols being typically more dangerous. The various effects of aerosol size distribution on solar radiation and health make it an important consideration in climate and air quality models (Gong et al., 2003) and an important source of uncertainty in radiative forcing calculation and attribution (Li et al., 2022; Zhang et al., 2024).

In this study, we used GRASP and AOD from PFR observations to retrieve the SD parameters. The aim is to assess the performance of such retrievals using only AOD at four wavelengths in the range of 368-862 nm. We also investigate the performance of GRASP retrievals under different conditions and aerosol types, as well as the effect of wavelength selection and spectral range.

## 2 Instruments and methodology

### 2.1 Instrumentation and locations

To validate aerosol properties retrieved from PFR AOD (GRASP-PFR hereafter), we chose four stations with several years of parallel CIMEL and PFR measurements. These stations also have different characteristics, so we could validate the retrievals under different conditions. The sites and time series are: Davos in Switzerland (2005-2022), Izaña in Tenerife, Spain (2004-2022), Hohenpeissenberg and Lindenberg in Germany (2013-2022).

Davos is a mountainous Alpine town in Central Europe with the station located at 1589 m above sea level (a.s.l.). Its atmosphere is generally pristine, with occasional intrusions of anthropogenic aerosols from the surrounding more densely populated areas and dust episodes from the Sahara Desert; hence, the seasonal patterns of AOD depend on the atmospheric circulation (Nyeki et al., 2012). The average AOD at 500 nm is below 0.1 (Nyeki et al., 2012; Karanikolas et al., 2022).

Izaña is a high-altitude site (2401 m a.s.l.) in the Canary Islands with a particularly clean atmosphere under background conditions, but there are several dust intrusions from the Sahara Desert leading to higher AODs. In Izaña, the AOD at 500 nm remains below 0.1 except during dust episodes that can lead to AOD > 0.5. Dust episodes are particularly frequent during July and August, when the number of days affected by them tend to exceed the number of days under background conditions (Barreto et al., 2022).

Hohenpeissenberg is a mountain station close to the Bavarian Alps at 989 m; hence, its characteristics are similar to those of Davos (low aerosol load, mostly fine particles), although its aerosol load is generally higher than that of Davos (Nyeki et al., 2012).

Finally, Lindenberg is a rural station in the region around Berlin in East Germany at an altitude of 120 m, so it is more affected by anthropogenic aerosols. It is expected to be more polluted than the other three stations and to include mostly fine particles (Doppler et al., 2024; Wacker et al., 2024).



### 2.1.1 PFR

The Precision Filter Radiometer (PFR), utilized by the GAW-PFR network (Wehrli, 2000), is designed to measure aerosol optical depth (AOD) and the Angström Exponent (AE). The instrument conducts direct solar irradiance (DSI) measurements every minute across four nominal wavelengths: 368, 412, 500, and 862 nm. It is mounted on an independent tracking system to ensure continuous alignment with the Sun throughout the day. The device features a quartz window at its entrance, protecting internal components from external environmental conditions. The internal environment of the PFR is stabilized by filling it with dry nitrogen at a pressure of approximately 2 bar. The temperature is maintained at 20°C with a precision of  $\pm 0.1^\circ\text{C}$  using a Peltier-controlled system. After sunlight passes through the quartz window, it is transmitted through interference filters, which isolate specific wavelengths with a bandwidth (full-width-at-half-maximum (FWHM)) of 3 to 5 nm before reaching a silicon photodiode detector. The instrument's field-of-view angle (FOV) at FWHM is approximately  $2^\circ$ . Measurements are performed as follows: every minute, the shutter opens for 10 seconds, during which 10 sequential measurements are taken at each wavelength. This setup minimizes filter degradation caused by prolonged exposure to solar radiation. Three PFRs in Davos (Switzerland) form the reference triad. Instruments at Mauna Loa (Hawaii) and Izaña (Tenerife) are calibrated using the Langley Plot method (Toledano et al., 2018; Kazadzis et al., 2018b) and serve as stability checks for the reference triad. Instruments from other stations are calibrated in Davos against the reference triad.

### 2.1.2 CIMEL

The CIMEL sun and sky photometer (Barreto et al. 2016; Giles et al., 2019), the primary instrument of the AERONET network, is used to measure AOD, AE, and a range of other columnar aerosol properties, including single scattering albedo (SSA) and size distribution (SD). The instrument is equipped with a two-axis robotic tracking system, enabling it to perform direct sun observations and sky radiance scans in multiple directions. The wavelengths measured vary by the instrument version, ranging from 340 nm to 1020 nm for some versions, while others extend up to 1640 nm. The maximum number of channels is 10. For this study, CIMEL instruments with at least eight filters were used, measuring at 340, 380, 440, 500, 675, 870, 940, and 1020 nm. The 940 nm channel specifically observes water vapour content. Filter bandwidths (FWHM) are typically 10 nm, except for 340 nm, 380 nm, and 1640 nm (2, 4, and 25 nm, respectively). The measurement process involves a rotating filter wheel, which moves to select filters sequentially, completing a full cycle in approximately 10 seconds. This process is repeated twice more, yielding three consecutive measurements (triplets) within 30 seconds. Triplet data are crucial for cloud screening (Smirnov et al., 2000; Giles et al., 2019). A silicon detector records the radiation, while the instrument's  $1.2^\circ$  FOV ensures precise solar alignment. To further enhance accuracy, a four-quadrant detector identifies the point of maximum solar intensity, ensuring the instrument points directly at the Sun. The instrument's schedule includes sky radiance scans at various scattering angles, which are used to retrieve aerosol properties at 440, 675, 870, and 1020 nm. AERONET provides public access to AOD data at three quality levels: Level 1.0 (unscreened), Level 1.5 (cloud-screened), and Level 2.0 (cloud-screened with final calibration and quality assurance).



### 195 2.1.3 BTS spectroradiometers

The BiTec Sensor (BTS) (Zuber et al., 2018; Zuber et al., 2021; Gröbner et al., 2023) consists of two array spectroradiometers, each measuring the spectral DSI in different spectral regions. The FoV of the instrument is 3° FWHM with 2° plateau. The first covers wavelengths from the ultraviolet (UV) to near-infrared (IR) in the range of 300-1050 nm with a spectral resolution of 2.5 nm at full width half maximum (FWHM) and measures the irradiance with a silicon detector. The second spectroradiometer extends the range to the near-IR by measuring from 950 to 2150 nm with a resolution of 8 nm and uses an extended InGaAs detector. For each of the two spectroradiometers, a collimator ensures the measurement of DSI only and a diffuser is used as the entrance optic. The spectroradiometers are mounted on a solar tracker to automatically follow the Sun. Both spectroradiometers include temperature stabilization to avoid the effect of the environment on the instrument's performance. The instrument is calibrated to provide irradiance measurements in SI units ( $\text{W}/\text{m}^2/\text{nm}$ ), which allows the retrieval of AOD using satellite-based top of the atmosphere solar irradiance. The calibration expanded uncertainty (at a 95% confidence coverage interval) decreases from 3% at 300 nm to 1.0% at 400 nm, remains at 1.0 % between 400 nm and 1400 nm and increases to 3% until 2150 nm. The AOD retrieval includes corrections for the absorption of ozone ( $\text{O}_3$ ). The wavelength channels at 1022.0, 1238.0, 1551.0, 2108.1 and 2129.8 nm were also corrected for the absorption of water vapour ( $\text{H}_2\text{O}$ ), carbon dioxide ( $\text{CO}_2$ ), methane ( $\text{CH}_4$ ) and nitrous oxide ( $\text{N}_2\text{O}$ ).

### 210 2.2 GRASP algorithm

GRASP (described in Dubovik et al., 2014 and Dubovik et al., 2021) is an inversion algorithm that uses the multi-term linear estimation techniques to retrieve aerosol properties from different types of observations (active and passive remote sensing instruments, both from ground-based and satellite instruments). In this study, we focus on the retrievals that require only AOD as input. AOD at more than one wavelength provides retrievals of the SD parameters ( $C_{\text{vf}}$ ,  $C_{\text{vc}}$ ,  $R_{\text{vf}}$ ,  $R_{\text{vc}}$ ,  $\sigma_{\text{vf}}$  and  $\sigma_{\text{vc}}$ ) as a main output, and other derived products such as  $\text{AOD}_f$  and  $\text{AOD}_c$  or total effective radius ( $R_{\text{eff}}$ ) or total volume concentration ( $C_{\text{VT}}$ ),  $\text{AOD}_f$  and  $\text{AOD}_c$ . Using the SD parameters, we can also compute  $C_{\text{VT}}$  and  $R_{\text{eff}}$  ([https://aeronet.gsfc.nasa.gov/new\\_web/Documents/Inversion\\_products\\_for\\_V3.pdf](https://aeronet.gsfc.nasa.gov/new_web/Documents/Inversion_products_for_V3.pdf), last access 23/12/2024).

GRASP requires a set of initial guesses for the parameters we intend to retrieve (in our case the SD parameters). The complex refractive index is not retrievable with only AOD as an input parameter, so it is required as an a-priori input parameter. GRASP includes a forward model to simulate the AOD observations using the SD parameters and refractive index, which can be run exclusively (for example, to perform tests with synthetic data). During the inversion process, GRASP first uses the initial guesses of the aerosol properties to simulate the AOD and compare it with the AOD observations. Through an iterative process,



it changes the combination of aerosol properties' values until it identifies the optimal solution through the maximum likelihood method.

## 225 2.3 Retrieval and validation methodology

To retrieve the SD parameters from PFR AOD, we used the multi-initial guesses approach described in Torres et al., (2017) and Torres and Fuertes, (2021) for the GRASP settings. We also used a modified version of the criteria in the same studies, to consider an inversion valid. To keep the inversions, the absolute inversion fitting error must be below 0.01 if the AOD at 412 nm is below 0.5 and below  $AOD_{412} \times 0.011 + 0.007$  if the AOD at 412 nm is above 0.5. The AOD absolute error at 500 nm has  
230 to be below  $0.01 + 0.005 \times AOD_{500}$ . We also kept only cases with AOD at 500 nm above 0.03 to ensure that there is at least some aerosol load. When comparing properties corresponding to the fine mode, we also kept only data corresponding to  $AOD_f > 0.02$  and  $AE > 0.3$ . For coarse mode properties, the thresholds are  $AOD_c > 0.02$  and  $AE < 1.8$ .

To validate the GRASP-PFR retrievals, we used the AERONET products as reference. For  $AOD_f$  and  $AOD_c$ , we used as reference both sky radiance inversions (AER-SKY) and the output of the spectral deconvolution algorithm (AER-SDA). The  
235 other parameters are available only through AER-SKY. The comparisons between GRASP-PFR and AER-SDA are point to point for coincident measurements with a maximum time difference of 30 seconds. On the other hand, the almucantar scans last approximately 5 minutes. Therefore, for the GRASP-PFR and AER-SKY comparisons, we used the median of all PFR measurements during a 5-minute period starting up to 30 seconds earlier or later from the almucantar scan starting time. Finally, to ensure a better quality of comparisons that more clearly display the performance of GRASP, we filtered the datasets  
240 according to their AOD differences (PFR – CIMEL and AER-SKY – AER-SDA),  $AOD_f$  and  $AOD_c$  (AER-SKY – AER-SDA). More details are available in the supplement section S1.

The retrieval of the SD parameters using AOD requires the prior knowledge (or assumption) of the complex refractive index as input to GRASP. The refractive index affects the retrievals, especially through an anticorrelation between the real part and the radii or concentrations (Van de Hulst, 1957; Yamamoto and Tanaka, 1969; King et., 1978; Torres et al., 2017). However,  
245 careful selection of the refractive index can reduce the retrieval error. In our case, since AERONET timeseries were available, we used as input the AER-SKY refractive index climatologies. However, such climatologies are not available in most of the GAW-PFR stations. Therefore, it is important to investigate the effect that a refractive index assumption may have on the GRASP-PFR retrievals. For this purpose, we selected two years of data from Izaña and Lindenberg and one year from Davos and Hohenpeissenberg to repeat the GRASP-PFR retrievals using only one value of refractive index for all sites and months.  
250 The fixed refractive index is 1.45 for the real part and 0.003 for the imaginary part. The AER-SKY climatologies we used at these stations vary in the range of 1.38-1.49 for the real part and 0.0005-0.0090 for the imaginary part (Sect. S3).

## 2.4 Methodology to investigate the spectral range effect

The PFR and CIMEL measure AOD over a limited spectral range at selected wavelengths. However, BTS spectroradiometers can provide a larger spectral range and resolution. One of our aims was to investigate the effect of using different wavelength



255 selections of spectral AOD to retrieve the SD parameters using GRASP. Taking advantage of the large range of BTS  
wavelengths, we selected sixteen wavelengths unaffected by strong gas absorption (so lower uncertainty of AOD retrieval)  
that increase the spectral range significantly compared to CIMEL, namely: 340.3, 367.9, 380.1, 412.1, 440.1, 500.4, 675.1,  
747.1, 780.4, 863.1, 869.9, 1022.0, 1238.0, 1551.0, 2108.1 and 2129.8 nm. We also use seven of them (the closest to the  
CIMEL channels: 340.3, 380.1, 440.1, 500.4, 675.1, 869.9 and 1022.0 nm) to repeat the GRASP retrievals and compare with  
260 the output of all sixteen wavelengths. BTS AOD was available in Davos since September 2021 and we used data until  
September 2024.

Any differences between the output of different wavelength selections may originate either from how GRASP responds to the  
input spectral range and resolution, or from noise and unusual spectral dependencies in AOD. To further investigate such  
effects, we repeated the retrievals for both wavelength selections using extrapolated AOD instead of the measured one  
265 according to the Angström law (Eq. 2). To extrapolate the AOD at the selected wavelengths, we used the logarithmic form of  
Eq. 2 and a least squares linear fit on the observed BTS AOD to retrieve the AE and turbidity coefficient for each spectrum.  
The wavelengths used for the linear fit are: 340.3, 367.9, 380.1, 412.1, 440.1, 500.4, 675.1, 863.1, 869.9 and 1022.0 nm. The  
final dataset includes only data corresponding to  $R^2 > 0.8$  and  $RMSE < 0.5$  for the linear fit. We also rejected data with  $R^2 < 0.8$   
from a least-squares power fit according to Eq. 2 using the same wavelengths and  $RMSE < 0.005$ . We compared the BTS AOD  
270 with the PFR AOD at the common wavelengths using a maximum 30-second threshold for time difference for the data to be  
considered coincident. We rejected all points corresponding to AOD differences  $> 0.07$  for 367.9 nm,  $> 0.05$  for 412.1 and 500.4  
nm and  $> 0.04$  for 863.1 nm.

As the aim of this study is to investigate the effects of wavelength selection, we did not focus on optimising a combination of  
several GRASP settings per inversion for each wavelength selection; rather, used two sets of initial guesses for the  
275 concentrations and radii per inversion, depending on AOD and AE and retained the inversion with the smallest residual. For  
all the other settings, we used fixed values.  $R_{vc}$  initial guesses were fixed to 1.75  $\mu\text{m}$ . The settings were selected according to  
self-consistency tests (Torres et al., 2017). The settings and more details about the procedure are available in Sect. S4. We  
filtered GRASP-BTS retrievals according to the inversion residual, as with the PFR (Sect. 2.3), but with some modification.  
Using more wavelengths results in larger residuals more easily. The same applies when using observed AOD in comparison  
280 to extrapolated AOD. Also, extrapolated AOD tends to show lower residuals compared to inversions from observed AOD.  
The criteria correspond to maximum values of the absolute inversion fitting error (abs-res) and the absolute error of AOD at  
500 nm (abs-res\_500). We present the thresholds for each case in Fig. 1. We also used AER-SKY level 1.5 data for the same  
period as reference. We also kept the AER-SKY data corresponding to an inversion sky residual  $< 7\%$  and a sun residual  $<$   
0.35% (optical residuals of the direct irradiance and sky radiance fitted by the model to the observations, described in  
285 [https://aeronet.gsfc.nasa.gov/new\\_web/Documents/Inversion\\_products\\_for\\_V3.pdf](https://aeronet.gsfc.nasa.gov/new_web/Documents/Inversion_products_for_V3.pdf)).

To compare the GRASP-BTS retrievals with AER-SKY, we used the median of all GRASP-BTS measurements within the  
time period from one minute before the start of the almucantar scan to six minutes after the scan's starting time. From the  
comparisons, we kept only data corresponding to AOD  $> 0.03$  at 500 nm. As for the case of GRASP-PFR, we kept only data



290 corresponding to  $AOD_f > 0.02$  and  $AE > 0.3$  when comparing fine mode parameters and  $AOD_c > 0.02$  and  $AE < 1.8$  for coarse mode parameters.

<b>AOD-obs – 7 wvl.</b>	$abs-res < 0.015 - \text{if } AOD_{440} < 0.5$ $abs-res < AOD_{440} \times 0.016 + 0.007 - \text{if } AOD_{440} > 0.5$ $abs-res_{500} < 0.01 + 0.005 \times AOD_{500}$
<b>AOD-ext – 7 wvl.</b>	$abs-res < 0.011 - \text{if } AOD_{440} < 0.5$ $abs-res < AOD_{440} \times 0.014 + 0.004 - \text{if } AOD_{440} > 0.5$ $abs-res_{500} < 0.009 + 0.005 \times AOD_{500}$
<b>AOD-obs – 16 wvl.</b>	$abs-res < 0.018 - \text{if } AOD_{440} < 0.5$ $abs-res < AOD_{440} \times 0.014 + 0.009 - \text{if } AOD_{440} > 0.5$ $abs-res_{500} < 0.018 + 0.005 \times AOD_{500}$
<b>AOD-ext – 16 wvl.</b>	$abs-res < 0.015 - \text{if } AOD_{440} < 0.5$ $abs-res < AOD_{440} \times 0.017 + 0.005 - \text{if } AOD_{440} > 0.5$ $abs-res_{500} < 0.012 + 0.005 \times AOD_{500}$

Figure 1: Schematic representation of the criteria to filter the GRASP-BTS retrievals for each wavelength selection and AOD calculation method.

## 295 3 Results

### 3.1 GRASP - PFR AOD retrievals

In this section, we describe the results of the validation of GRASP-PFR against AER-SKY and AER-SDA for the full time-series of the four stations and how the differences in the aerosol properties behave under different conditions.

#### 3.1.1 Validation of GRASP - PFR AOD inversions

300 In this section, we present the validation of retrievals of aerosol SD parameters by GRASP-PFR. First, we show that the AOD comparison between PFR and CIMEL for the selected data show excellent agreement for each station, as all median differences and standard deviations are below 0.01 (Table 1). The comparisons between GRASP-PFR and AER-SKY for  $AOD_f$  and  $AOD_c$  at 500 nm show excellent agreement as well (Fig. 2). For  $C_{VT}$ , we obtained larger relative differences and slope of the linear

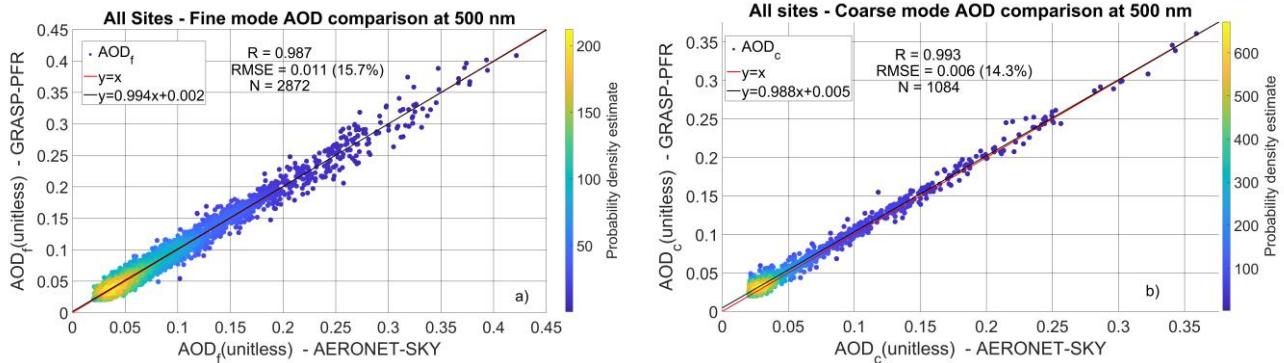


fit between the datasets, but the correlation remained excellent ( $R > 0.95$ ) (Fig. 3a).  $R_{\text{eff}}$  also shows good correlation ( $R > 0.8$ ),  
 305 but with larger variance and deviation of the slope from 1 ( $> 1.5$ ) (Fig. 3b).  $\text{AOD}_f$  also shows similar results when compared  
 to AER-SDA output ( $R = 0.99$  median difference 0.005 and standard deviation 0.01 across 151415 common selected  
 measurements, Sect. S1). In Table 2, we show the statistics of the comparisons for all parameters (median differences, standard  
 deviations and correlation factors); more information is in Figs. S1-S2, where we show the comparisons of  $C_{Vf}$ ,  $C_{Vc}$  between  
 GRASP-PFR and AER-SKY as well as the  $\text{AOD}_f$  and  $\text{AOD}_c$  comparisons with AER-SDA. In summary, the concentrations  
 310 show larger correlation factors than the radii. However,  $C_{Vc}$  shows the largest relative median difference and  $R_{\text{eff}}$  the smallest.  
 Also,  $R_{\text{eff}}$  shows the largest relative standard deviation and  $R_{Vf}$  the smallest.

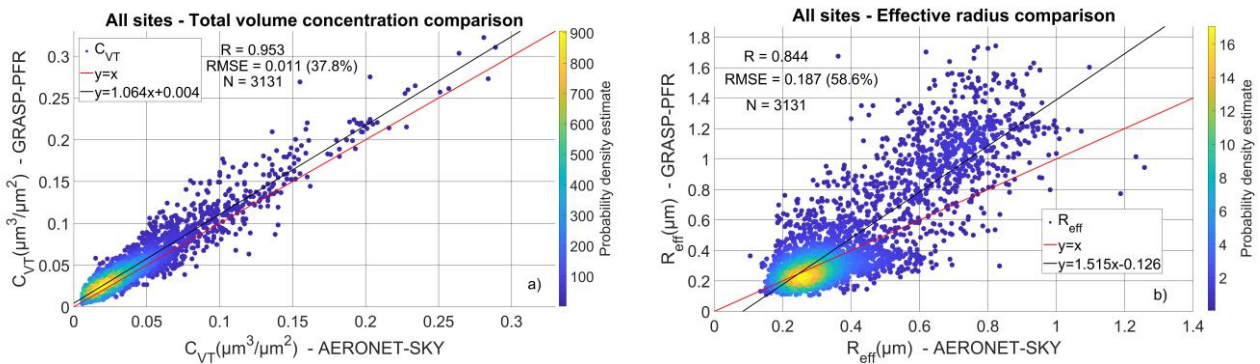
The uncertainties of the inverted parameters vary depending on the conditions. AERONET provides point-to-point uncertainty  
 for two of the SD parameters ( $R_{Vf}$  and  $R_{Vc}$ ). It also provides the root mean square error (RMSE) for  $\text{AOD}_f$  and  $\text{AOD}_c$  (O' Neill  
 et al., 2003) corresponding to the AER-SDA retrievals. For  $\text{AOD}_f$ , 78% of the differences between GRASP-PFR and AER-  
 315 SDA are within the RMSE. For  $\text{AOD}_c$ , the same percentage is 85%. On the other hand, for  $R_{Vf}$  the differences between GRASP-  
 PFR and AER-SKY within the uncertainties account for only 15% of the points and 10% for  $R_{Vc}$ .

Table 1: AOD differences at 500 nm between PFR and CIMEL (AER-SKY retrieved from almucantar scans and AER-DIR  
 from direct sun) for each one of selected stations. The AOD comparison with AER-SKY includes the data selected for GRASP-  
 PFR – AER-SKY comparisons of aerosol SD parameters and the comparison with AER-DIR the data selected for GRASP-  
 320 PFR – AER-SDA comparisons of  $\text{AOD}_f$  and  $\text{AOD}_c$ .

Location	Median difference	St.d.	P95-P5	median PFR	AOD	Number of measurements
<b>PFR - AER-SKY</b>						
Davos	0.002	0.005	0.015	0.068		266
Hohenpeissenberg	0.007	0.006	0.018	0.098		960
Izaña	0.000	0.005	0.017	0.073		895
Lindenberg	0.001	0.008	0.024	0.119		1010
<b>PFR – AER-DIR</b>						
Davos	0.001	0.005	0.016	0.053		49904
Hohenpeissenberg	0.006	0.006	0.019	0.077		36753
Izaña	0.002	0.004	0.012	0.036		96236
Lindenberg	0.002	0.007	0.021	0.120		31522



325 **Figure 2: Scatter plot of  $AOD_f$  (a) and  $AOD_c$  (b) for the GRASP-PFR and AER-SKY retrievals from all four locations. The plots include the correlation factor (R), the root mean square error (RMSE) and the number of observations (N). The colour bar shows the density of the points. We also include the linear fit between the datasets and the  $y=x$  line.**



330 **Figure 3: Scatter plot of  $C_{VT}$  (a) and  $R_{eff}$  (b) for the GRASP-PFR and AER-SKY retrievals from all four locations. The plots include the correlation factor (R), the root mean square error (RMSE) and the number of observations (N). The colour bar shows the density of the points. We also include the linear fit between the datasets (black line) and the  $y=x$  (red) line.**

Table 2: Statistics of the differences between GRASP-PFR retrievals and AER-SKY. We also include the AOD at 500 nm comparison between the PFR and AER-SKY. We also include the correlation factor (R) and the relative median difference compared to the median of each parameter from the reference dataset (PFR for AOD, AER-SKY for every other parameter).

Parameter	Median difference	St.d.	R	Relative median difference (%)	median of the parameter	Number of measurements
AOD 500 nm	-0.002	0.007	0.99	-2.1	0.094	3131
AOD <sub>f</sub> 500 nm	-0.001	0.011	0.98	-1.4	0.070	2872
AOD <sub>c</sub> 500 nm	-0.003	0.007	0.99	-7.1	0.042	1084
$C_{VT}$	-0.006	0.012	0.95	-20.7	0.029	3131

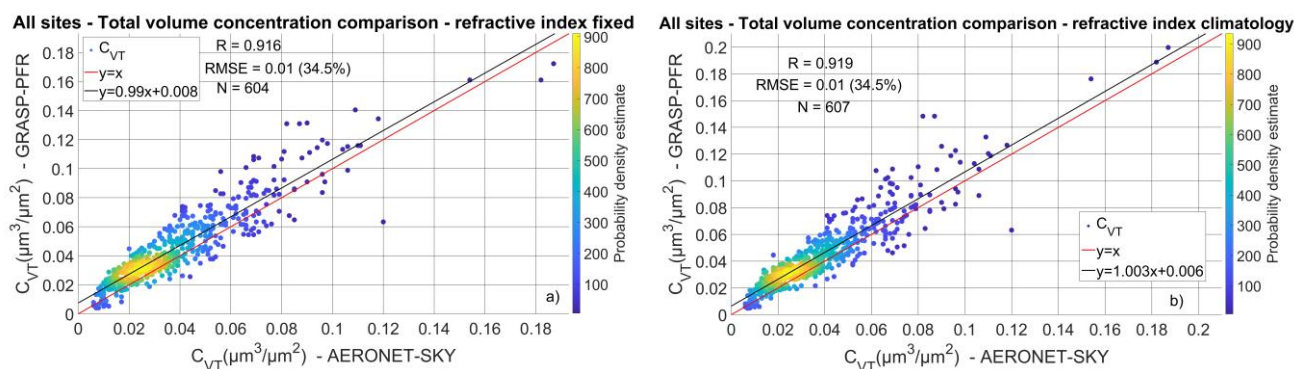


$C_{Vf}$	-0.001	0.006	0.88	-9.1	0.011	2872
$C_{Ve}$	-0.010	0.015	0.96	-27.8	0.036	1084
$R_{eff}$	-0.012	0.213	0.84	-3.8	0.319	3131
$R_{Vf}$	0.014	0.038	0.40	8.3	0.168	2872
$R_{Ve}$	-0.281	0.503	0.47	-15.3	1.835	1084

335 **3.1.2 Effect of refractive index on the PFR AOD inversions**

In this section, we show the performance of the comparisons between GRASP-PFR and AER-SKY retrievals for different refractive index selections (one fixed value in panel against climatology per site) (Table 3), including an example of scatter plots regarding  $R_{eff}$  (Fig. 4). The comparisons between GRASP-PFR and AER-SKY (during common years) tend to show better agreement when using the refractive index climatology, as expected, but the differences are very small (Table 3, Fig. 3).

340 In Table 3, we summarize the results for all parameters (differences between the statistics of the GRASP-PFR – AER-SKY comparisons for each refractive index selection). The results show that the effect of the refractive index is small for the refractive index selections we used in this study. Most differences of the median differences between GRASP-PFR and AER-SKY in the two refractive index cases are close to 0. The differences in the correlation coefficients ( $\Delta R$ ) and the differences in the standard deviations ( $\Delta St.d.$ ) are also very small ( $\Delta R \leq 0.04$ ).  $\Delta St.d.$  is smaller than the St.d. of the same parameter in Table 345 2 and typical uncertainty values of the four available parameters (Sect. S1).



350 **Figure 4: Scatter plot of  $C_{VT}$  for the GRASP-PFR and AER-SKY retrievals from all four locations for a fixed value of refractive index (a) and the use of refractive index climatologies (b). The plots include the correlation factor (R), the root mean square error (RMSE) and the number of observations (N). The colour bar shows the density of the points. We also include the linear fit between the datasets and the  $y=x$  line.**



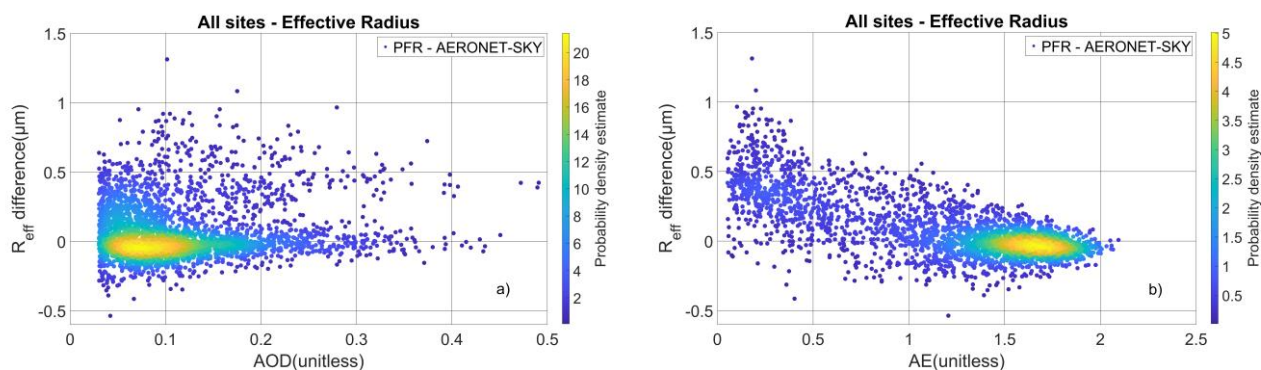
355 Table 3: Statistics of the differences between the GRASP-PFR retrievals and AER-SKY comparisons for different refractive index selections, including R and the median of each parameter from AER-SKY retrievals.

Parameter	Difference of the median difference	$\Delta$ St.d.	$\Delta$ R	median of the parameter	Number of measurements
AOD <sub>f</sub>	0.000	-0.004	-0.009	0.070	605
AOD <sub>c</sub>	0.000	-0.001	-0.008	0.042	159
C <sub>V<sub>T</sub></sub>	0.001	0.000	-0.011	0.029	604
C <sub>V<sub>f</sub></sub>	0.001	0.001	-0.003	0.011	605
C <sub>V<sub>c</sub></sub>	0.001	0.001	0.011	0.036	159
R <sub>eff</sub>	0.002	0.000	-0.014	0.319	604
R <sub>V<sub>f</sub></sub>	0.004	-0.001	-0.001	0.168	605
R <sub>V<sub>c</sub></sub>	-0.019	0.016	-0.037	1.835	159

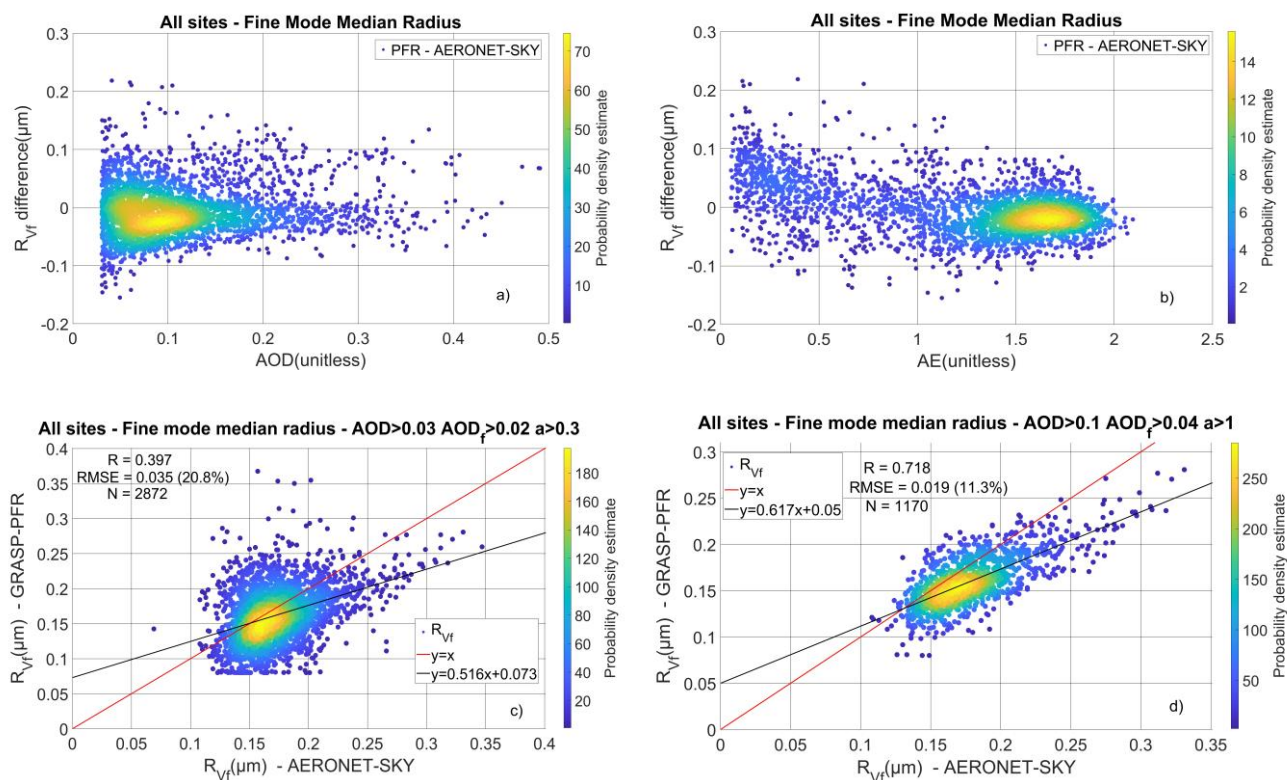
### 3.1.3 Sensitivity of the retrieval of aerosol properties to the aerosol conditions

In general, aerosol properties inversions tend to be more accurate at higher AODs (Sinyuk et al., 2020). In Sects. 3.1.1 and 3.1.2, we showed that GRASP-PFR performed well for the AOD modal separation and concentrations even under particularly low AOD conditions (AOD at 500 nm below 0.05). In this section, we show that the radii can be improved by further restricting the datasets to more specific conditions.

As aerosol load and size depend on AOD and AE, we could expect that the retrieval of aerosol properties should improve at higher AOD, as well as higher AE for small aerosols (fine mode) and lower AE for larger aerosols (coarse mode). In Fig. 5, we show that the R<sub>eff</sub> differences increase at very low AODs, but mostly at low AEs (particularly below 1, where we observe a positive bias towards larger GRASP-PFR values). The same phenomenon is evident for R<sub>V<sub>f</sub></sub> as well (Fig. 6a and 6b). By further restricting the dataset (AOD at 500 nm > 0.1, AOD<sub>f</sub> > 0.04 and AE > 1), we achieved a significant improvement in R<sub>V<sub>f</sub></sub> in terms of correlation and RMSE of the linear fit between GRASP-PFR and AER-SKY (scatter plots in Fig. 6c and 6d). There was also improvement for R<sub>eff</sub>, but not for R<sub>V<sub>c</sub></sub> (Table S1).



370 **Figure 5: The  $R_{eff}$  difference between GRASP-PFR and SKY-AER in relation to AOD (a) and AE (b).**

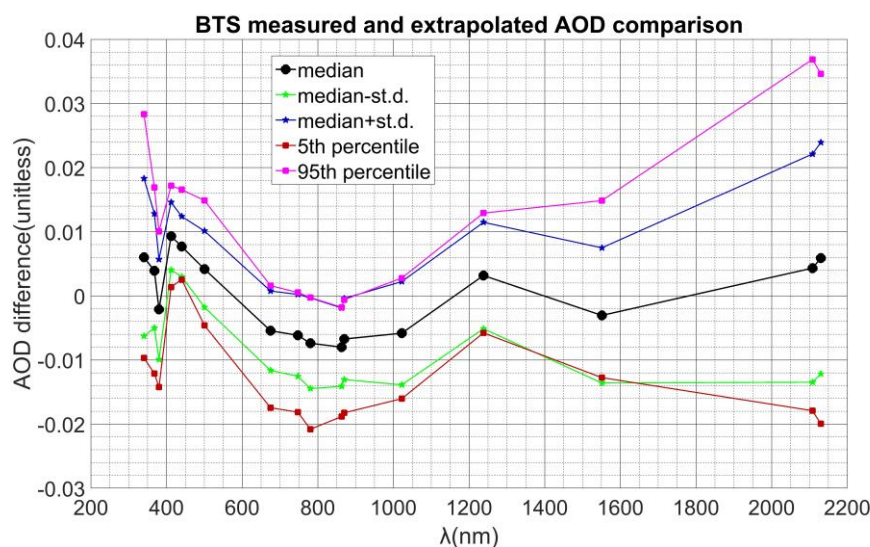


375 **Figure 6: The  $R_{Vf}$  difference between GRASP-PFR and SKY-AER in relation to AOD (a) and AE (b). Also, scatter plots for  $R_{Vf}$  from GRASP-PFR and AER-SKY (c and d) under different thresholds of AOD and AE in data screening. In panel d) we have increased the AOD, AOD<sub>f</sub> and AE thresholds, which improved the comparison. All graphs correspond to all four locations.**



### 3.2 Effect of AOD spectral range

In this section, we present the results of the sensitivity study to the wavelength selection for GRASP-BTS retrievals. In Fig. 7, we show the deviations of observed BTS AOD (AOD-obs) from the extrapolated AOD using Eq. 2 (AOD-ext). The median AOD differences are  $<0.01$  for all wavelengths. However, there are cases (especially in the UV or IR) where the deviation is  $>0.02$ , either due to noise in the observed AOD or because aerosol conditions cause the AOD spectral dependence to deviate significantly from the Ångström law.

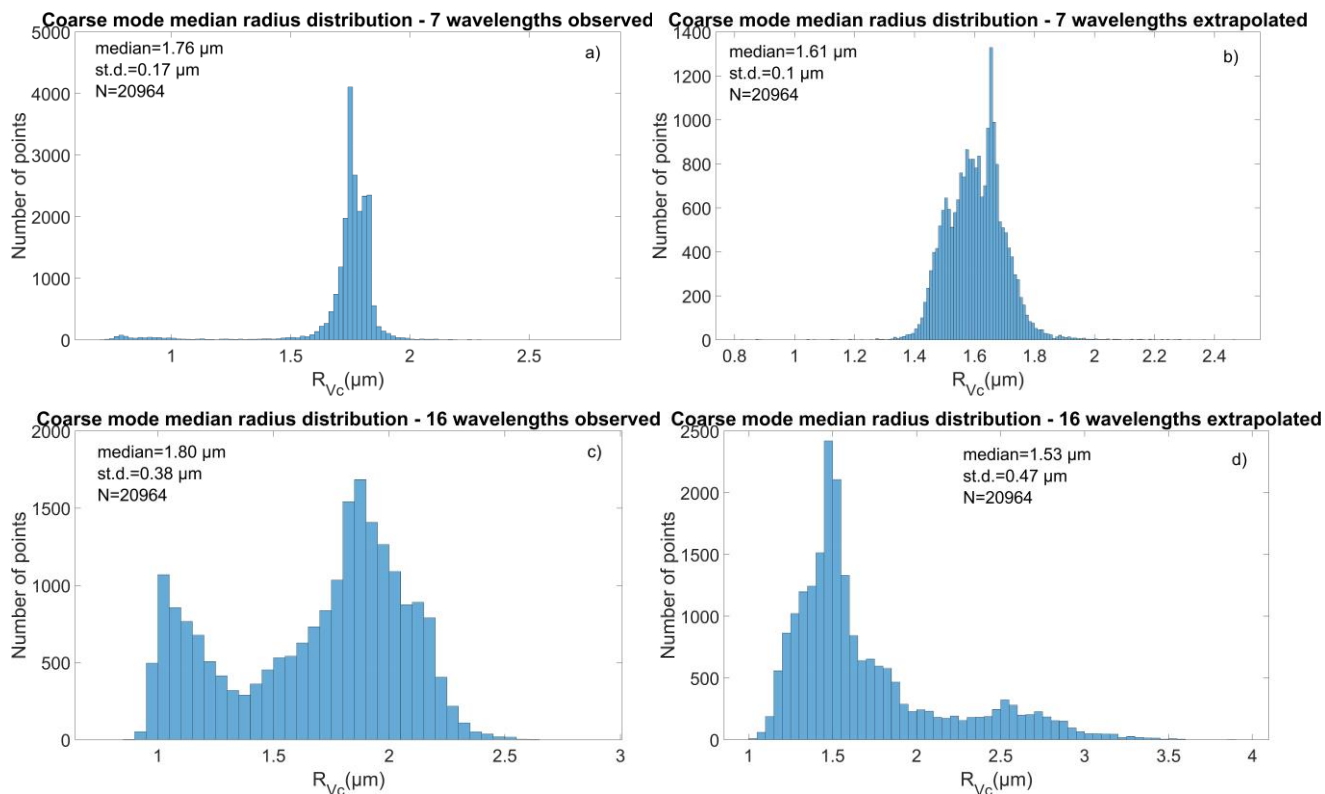


385

**Figure 7: The statistics of the differences between the BTS observed AOD and BTS AOD extrapolated using the Angström law.**

As we know from Torres and Fuertes, (2021) and as we show in Sects. 3.1 and 3.3,  $R_{V_c}$  showed low sensitivity to AOD. However, the coarse mode is generally more sensitive to longer wavelengths. Indeed, using the selection of sixteen wavelengths that cover the BTS spectral range, we see that the distribution of  $R_{V_c}$  output of GRASP-BTS shows larger variance compared to the seven wavelengths in the range 340-1022 nm (Fig. 8). However, the median  $R_{V_c}$  shows only a small difference between the wavelength selections and depends more on whether we used as input the AOD as measured by the instrument or fitted to Eq. 2 (AOD-obs or AOD-ext, described in Sect. 2.4).

390



395 **Figure 8: Histograms of the  $R_{Vc}$  GRASP-BTS retrievals using observed AOD at 7 wavelengths (a), extrapolated AOD at 7 wavelengths (b), observed AOD at 16 wavelengths (c), extrapolated AOD at 16 wavelengths (d).**

As shown in Table 4 (statistics of the differences between the GRASP-BTS retrievals), all four AOD datasets produced different GRASP-BTS output for all SD parameters. The largest standard deviation for most parameters is between the GRASP-BTS retrievals from AOD-obs at seven wavelengths and AOD-ext at sixteen wavelengths, which is expected. The median differences vary by parameter and we see no wavelength selection showing consistently larger or lower biases compared to the others.

The comparison of all four GRASP-BTS datasets with AER-SKY includes a particularly small number of measurements due to low data availability of AER-SKY data and low AOD in Davos, particularly in the coarse mode. The differences between GRASP-BTS and AER-SKY are not consistently smaller or larger for the same wavelength selection (statistics shown in Tables 5-6 for all parameters and AOD datasets), but in general tend to be smaller more often than not when we used the seven-wavelength selection. For the radii, the smallest standard deviations between GRASP-BTS and AER-SKY appear in the comparison with the retrievals from AOD-obs at sixteen wavelengths. For  $R_{Vc}$ , the correlation factor also increases when using sixteen wavelengths, from 0.46 to 0.60. However, the median differences of  $R_{eff}$  and  $R_{Vc}$  are larger compared to the retrievals from AOD-obs at seven wavelengths (Tables 5-6). The latter showed smaller median differences and standard deviations for



410 AOD<sub>c</sub> and C<sub>Vc</sub> as well. The correlation factors for the parameters other than R<sub>Vc</sub> are similar and depend on the parameter for which wavelength selection they are larger (Tables 5-6).

The GRASP-BTS comparisons with AER-SKY showed good consistency with the findings of the GRASP-PFR and AER-SKY comparison, despite the different instruments and datasets. Comparing the median differences, St.d. and R in Tables 5 and 6 to the corresponding from Table 2, we find that:

415 The correlation factors for C<sub>Vf</sub>, C<sub>Vc</sub>, R<sub>Vf</sub> and R<sub>Vc</sub> differ by 0.09 and 0.22 between the GRASP-PFR – AER-SKY and GRASP-BTS – AER – SKY comparisons, depending on the BTS AOD dataset, except for R<sub>Vf</sub> retrieved from AOD-ext ( $\Delta R = -0.86$  for seven wavelengths and  $\Delta R = -0.96$  for sixteen wavelengths). For the other parameters, they differ by less than 0.1.

For AOD<sub>f</sub> and AOD<sub>c</sub>, all absolute median and st.d. of differences, differ by no more than 0.011 between the GRASP-PFR – AER-SKY and GRASP-BTS – AER – SKY comparisons regardless of the BTS AOD dataset.

420 For the remaining parameters, the absolute relative median and st.d. of the differences, differ by 0% and 49%, depending on the parameter and BTS AOD dataset. In all parameters except C<sub>VT</sub>, C<sub>Vf</sub> and R<sub>eff</sub>, using AOD-obs at seven wavelengths shows better consistency of median differences between the GRASP-PFR and GRASP-BTS comparisons with AER-SKY. The same is true for the st.d. except for the comparisons of R<sub>Vf</sub>. AOD-obs at seven wavelengths also yielded the smallest  $\Delta R$  between the aforementioned comparisons (either alone or tied with another dataset) for all parameters except C<sub>Vf</sub> and R<sub>Vf</sub> (where it  
425 yielded the second smallest  $\Delta R$ ). This is expected, as the PFR also measures AOD with a spectral range and resolution closer to the seven-wavelength selection and the BTS AOD was filtered according to the comparisons of AOD-obs from each instrument.

430 Table 4: Statistics of the differences between the GRASP-BTS retrievals using 7 wavelengths and the observed AOD and GRASP-BTS retrievals for different selections of AOD. The first row of data shows the comparison of the AOD at 500 nm calculated by the GRASP forward model using the final solution of aerosol properties inversion between the GRASP-BTS retrievals using 7 wavelengths and the observed AOD and GRASP-BTS retrievals for different selections of AOD.

Parameter	7 wavelengths extrapolated		16 wavelengths observed		16 wavelengths extrapolated		Number of measurements
	median difference	St.d.	median difference	St.d.	median difference	St.d.	
AOD fitted	-0.002	0.004	0.000	0.001	-0.002	0.004	18948
AOD <sub>f</sub>	-0.013	0.011	-0.003	0.009	-0.010	0.015	18860
AOD <sub>c</sub>	0.008	0.009	0.003	0.009	0.004	0.014	8592
C <sub>VT</sub>	0.002	0.008	0.004	0.015	0.004	0.014	18948
C <sub>Vf</sub>	0.001	0.002	-0.001	0.001	0.001	0.003	18860
C <sub>Vc</sub>	-0.003	0.008	0.004	0.022	0.002	0.017	8592
R <sub>eff</sub>	-0.074	0.087	0.093	0.146	-0.046	0.124	18948
R <sub>Vf</sub>	-0.051	0.044	0.000	0.015	-0.038	0.063	18860
R <sub>Vc</sub>	-0.114	0.169	0.009	0.383	0.159	0.539	8592



435

Table 5: Statistics of the differences between the GRASP-BTS retrievals using different selections of AOD and the AER-SKY retrievals for seven wavelengths in the 340-1022 nm range. The first row of data shows the comparison of the AOD at 500 nm corresponding to the AER-SKY inversions and the AOD measured by BTS.

Parameter	7 wavelengths observed			7 wavelengths extrapolated			Number of measurements
	median difference	St.d.	R	median difference	St.d.	R	
AOD obs.	0.006	0.010	0.99	0.006	0.010	0.99	81
AOD <sub>f</sub>	-0.001	0.010	0.96	-0.012	0.009	0.96	80
AOD <sub>c</sub>	0.001	0.006	0.99	0.009	0.004	1.00	27
C <sub>VT</sub>	0.000	0.017	0.94	0.005	0.020	0.93	81
C <sub>Vf</sub>	-0.004	0.005	0.68	-0.002	0.005	0.66	80
C <sub>Vc</sub>	0.007	0.026	0.89	0.006	0.030	0.86	27
R <sub>eff</sub>	0.082	0.210	0.87	0.037	0.165	0.88	81
R <sub>Vf</sub>	0.019	0.051	0.23	-0.036	0.058	-0.46	80
R <sub>Vc</sub>	0.238	0.530	0.46	0.144	0.549	0.12	27

Table 6: Statistics of the differences between the GRASP-BTS retrievals using different selections of AOD and the AER-SKY retrievals for sixteen wavelengths in the 340-2130 nm range. The first row of data shows the comparison of the AOD at 500 nm corresponding to the AER-SKY inversions and the AOD measured by BTS.

Parameter	16 wavelengths observed			16 wavelengths extrapolated			Number of measurements
	median difference	St.d.	R	median difference	St.d.	R	
AOD obs.	0.006	0.010	0.99	0.006	0.010	0.99	81
AOD <sub>f</sub>	-0.007	0.009	0.96	-0.009	0.015	0.87	80
AOD <sub>c</sub>	0.006	0.015	0.98	-0.008	0.013	0.99	27
C <sub>VT</sub>	0.000	0.022	0.97	0.006	0.019	0.94	81



$C_{Vf}$	-0.005	0.005	0.65	-0.001	0.004	0.78	80
$C_{Vc}$	-0.008	0.027	0.93	0.023	0.028	0.87	27
$R_{eff}$	0.167	0.098	0.85	0.022	0.280	0.88	81
$R_{Vf}$	0.019	0.042	0.27	-0.035	0.101	-0.56	80
$R_{Vc}$	-0.459	0.452	0.60	0.761	0.720	-0.04	27

440

### 3.3 Case studies for different aerosol types

In this section we focus on case studies of two aerosol types. First, we assess the performance of GRASP-PFR under conditions where the predominant aerosol type is dust. We accomplish this by focusing on the Izaña site, where conditions are typically pristine except during dust episodes. Secondly, we focus on a highly unusual episode of long-range transport biomass burning smoke from the Canadian wildfires during the record-breaking year 2023 (Jain et al., 2024).

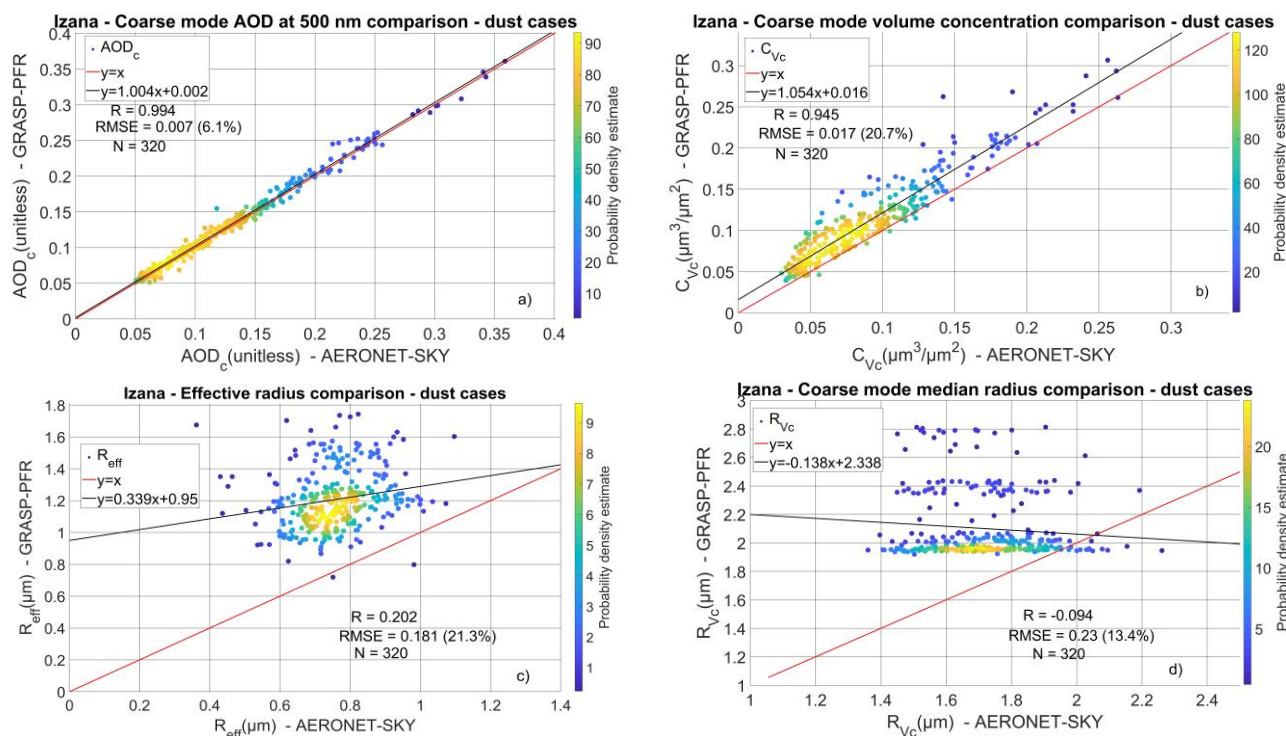
445

#### 3.3.1 Dust

According to Barreto et al. (2022), values of  $AE < 0.5$  correspond to aerosol conditions dominated by dust or mixed cases. As dust is the main coarse-particle type in Izaña, restricting the dataset to  $AE < 0.5$ ,  $AOD_c > 0.05$  and fine mode fraction (FMF)  $AOD_f/AOD < 0.35$  should yield cases where dust is a significant part or even the predominant part of the total aerosol load.

450 Therefore, we compared SD properties between GRASP-PFR and AER-SKY under these conditions. We summarize the results in Fig. 9 that includes the GRASP-PFR – AER-SKY scatter plots for  $R_{eff}$  and coarse mode parameters.  $AOD_c$  shows excellent agreement and  $C_{Vc}$  shows excellent correlation, though with some overestimation by from GRASP-PFR (Fig. 9 a and b).  $R_{Vc}$  showed no improvement compared to the general case (Fig. 9 c).  $R_{eff}$  showed worse performance compared to the general case, as expected from the findings in Sect. 3.1.4. This can be explained by the fact that we found better performance

455 for  $R_{Vf}$  than  $R_{Vc}$  and improvement under more restricted data. Therefore, under conditions where fine mode aerosol types are dominant, errors in  $R_{Vc}$  affect  $R_{eff}$  less, since  $R_{eff}$  is more influenced by  $R_{Vf}$ . In conditions of mostly coarse particles (and thus larger  $R_{eff}$ ), errors in  $R_{Vc}$  affect  $R_{eff}$  more significantly.



460

**Figure 9: Scatter plot of  $AOD_c$  (a),  $C_{Vc}$  (b),  $R_{eff}$  (c) and  $R_{Vc}$  (d) for the GRASP-PFR and AER-SKY retrievals in Izaña corresponding to  $AE < 0.5$ ,  $AOD_c > 0.05$  and  $FMF < 0.35$  (which leads to large dust proportion in the overall aerosols).**

$R_{Vc}$  generally, shows very low sensitivity to AOD as expected (Torres and Fuertes, 2021). The GRASP-PFR  $R_{Vc}$  retrievals usually do not deviate significantly from the initial guesses, leading to very small parameter variation that is not present in the  
 465 AER-SKY data (Fig. 9). Therefore, the multi-initial guess approach is not necessarily optimal for this parameter. Using prior knowledge for the GRASP-PFR retrievals -specifically a single initial guess for  $R_{Vc}$ - may improve the results. Accordingly, we repeated the retrievals shown in Fig. 9 using the median  $R_{Vc}$  from AER-SKY data ( $1.71 \mu m$ ) as the initial guess. The results are presented in Fig. 10 that includes the same graphs as Fig. 9 using the single  $R_{Vc}$  initial guess approach. The  $AOD_c$  comparison shows no significant differences. The  $C_{Vc}$  from GRASP-PFR is no longer systematically biased to larger values  
 470 compared to AER-SKY.  $R_{eff}$  remains biased to larger values, but the bias is reduced (intercept reduced from 0.95 to 0.74, RMSE from 21.3% to 13.4%) and  $R_{Vc}$  is closer to AER-SKY as well (intercept reduced from 0.95 to 0.74 and RMSE from 13.4% to 3.6%).



475

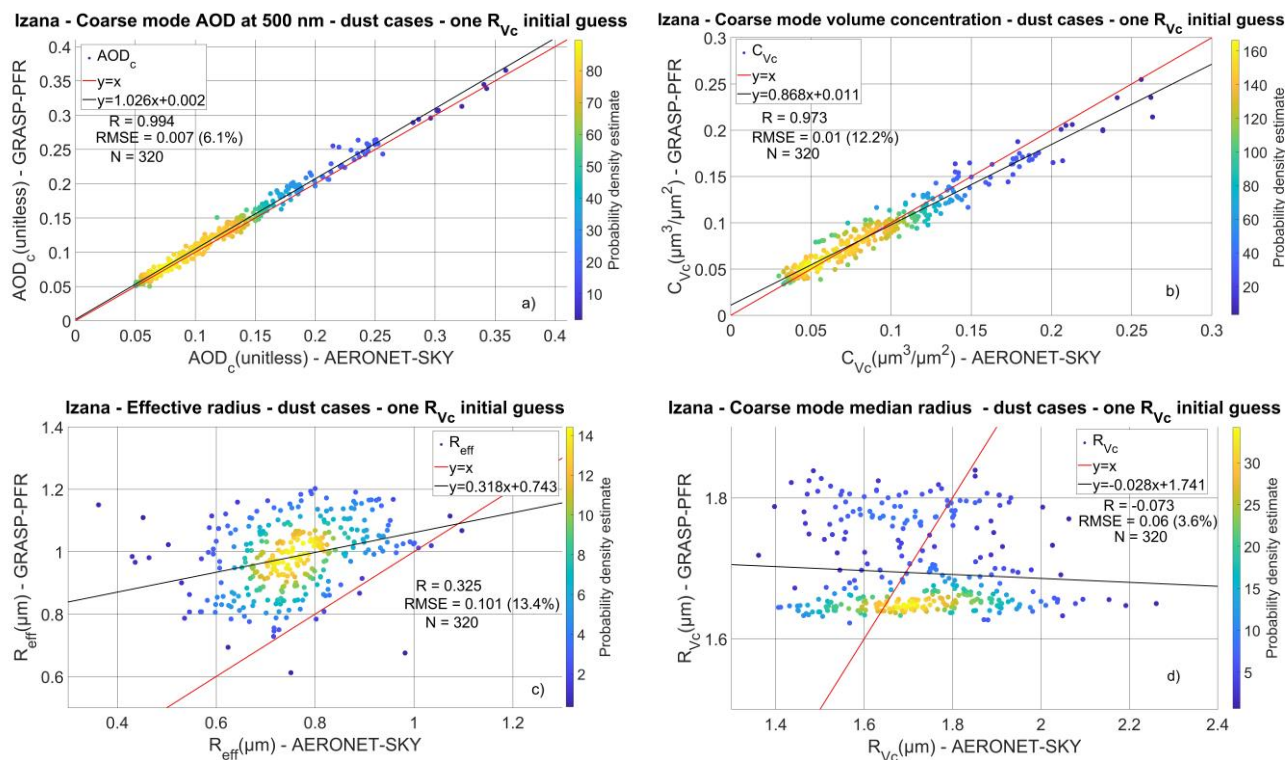


**Figure 10: Scatter plot of  $AOD_c$  (a),  $C_{Vc}$  (b),  $R_{eff}$  (c) and  $R_{Vc}$  (d) for the GRASP-PFR and AER-SKY retrievals in Izaña corresponding to  $AE < 0.5$ ,  $AOD_c > 0.05$  and  $FMF < 0.35$  and GRASP runs under one initial guess of  $R_{Vc}$ .**

480 **3.3.2 Smoke episode from Canadian wildfires**

During late September to early October 2023, long-range transport of smoke from the Canadian wildfires caused unusual AOD observations, where the highest AOD occurred at 500 nm rather than the shortest available wavelength, leading to negative AE in the UV and, in some cases, part of the visible spectrum. In Davos on 1 October 2023, this phenomenon was pronounced and observed by three different instruments (PFR, CIMEL, and BTS) (Fig. 11). In this section, we examine the SD characteristics associated with such aerosols and the extent to which GRASP retrievals using only AOD as input can reproduce those characteristics.

485

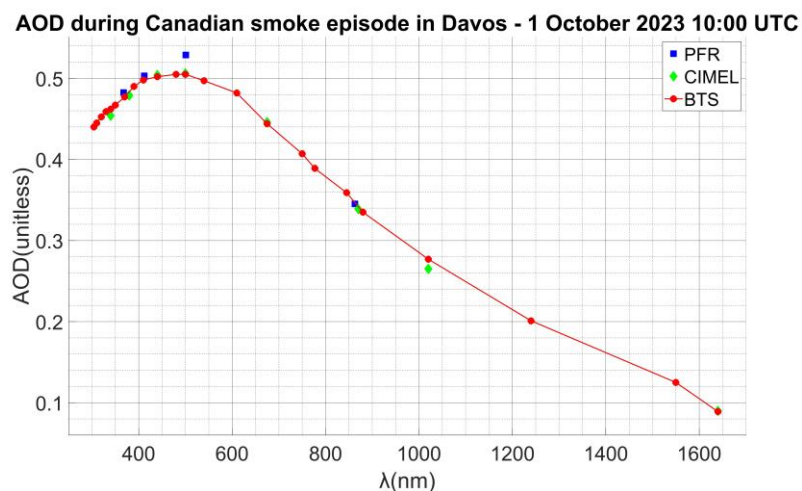


**Figure 11: The PFR, CIMEL and BTS AOD during a measurement of the unusual smoke episode in Davos during 1st of October 2023.**

490 During the smoke episode, we found two AERONET SD retrievals within 30 seconds of BTS and PFR AOD measurements. The SD shows that the vast majority of aerosols correspond to the fine mode, with a particularly high concentration and relatively narrow distribution. Moreover, the fine mode corresponds to unusually large radii (peak  $> 0.3 \mu\text{m}$ ) as shown in the SDs of Fig. 12. Similar AOD behaviour was observed during the 2020 California wildfires, with similar SD characteristics (Eck et al., 2023).

495 To retrieve the SD from AOD, we did not use the Torres and Fuertes, (2021) settings approach, since the low AE in that episode led to settings more appropriate for dust cases. The resulting output included strong overestimation of  $C_{Vc}$  when  $AOD_e > 0.2$  at 500 nm and inversion residuals larger than our selection thresholds. Both AER-SKY and AER-SDA outputs showed  $AOD_c < 0.003$  during that smoke episode. Using single retrievals with more general settings (Supplement Sect. S5), we reproduced the aforementioned SD characteristics for both PFR and BTS AOD. For BTS, we used a different wavelength  
500 selection than in Sect. 3.2 to include additional UV channels due to the unusual AOD behaviour. However, both PFR- and BTS-based retrievals—regardless of AOD source—showed overestimation of  $C_{Vf}$  and  $R_{Vf}$  compared to AERONET (Fig. 12). PFR AOD led to higher  $C_{Vf}$ , due to the higher AOD at 500 nm (Fig. 11). CIMEL AOD yielded similar results to BTS for coincident measurements (Fig. S4). We observed similar episodes at several AERONET stations. One of them (Narsarsuaq in Greenland) included CIMEL AOD with a pronounced peak at wavelength above 340 nm (Fig. 13a) and SD observations within  
505 1–8 minutes and low sky-radiance inversion residuals for AERONET SD ( $< 5\%$ ; Holben et al., 2006). Retrieving SD with GRASP using CIMEL AOD and the same settings, we again reproduced the SD characteristics and overestimated  $C_{Vf}$  and  $R_{Vf}$  (Fig. 13b).

Finally, we tested the effect of wavelength selection on SD retrievals using only BTS AOD. We applied four wavelength selections (Sect. S5): two spanning UV to near-IR, one excluding UV wavelengths, and one excluding IR wavelengths. All



510 selections yielded similar SDs. Excluding UV resulted in a larger  $C_{Vf}$  difference compared to the others, but the difference remained small (Fig. 12).

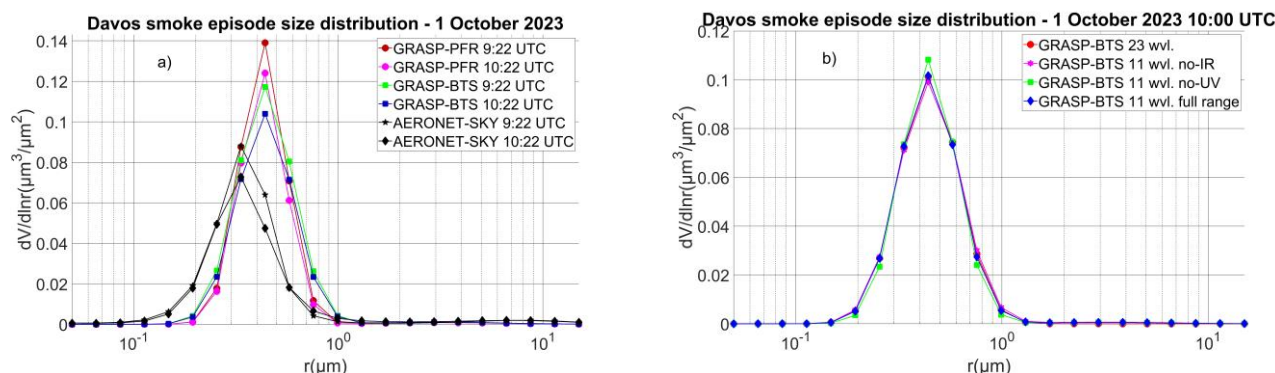
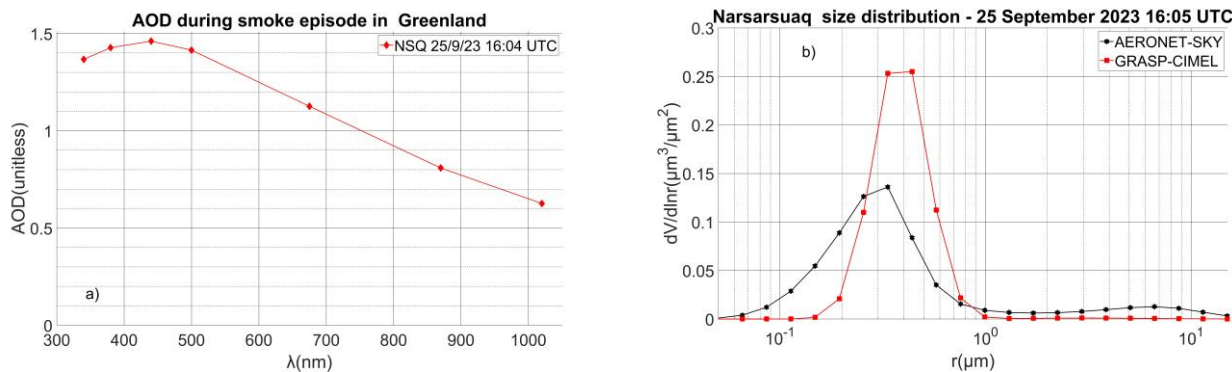


Figure 12: The SDs of AERONET (black lines) and GRASP retrievals (coloured lines) from PFR and BTS for two different common measurements (a) and the BTS retrievals for different wavelength selections (b).



515

Figure 13: (a) CIMEL AOD per wavelength at Narsarsuaq during the record-breaking Canadian wildfires. (b) GRASP-CIMEL size distribution retrievals (red lines) and the closest AERONET size distributions (black lines) at Narsarsuaq (b) during the record-breaking Canadian wildfires.

#### 4 Discussion

520 In the previous sections, we explored the capabilities of retrieving bimodal aerosol SD parameters using only AOD observations and the inversion model GRASP. In the first part of the study (Sects. 3.1.1, 3.1.2 and 3.1.3), we validated the GRASP-PFR retrievals against AERONET products (AER-SKY and AER-SDA). Our main findings are consistent with the validation study of Torres and Fuertes, (2021), which used AERONET AOD to retrieve SD parameters with GRASP. Of course, differences arise owing to the different locations and datasets. Torres and Fuertes, (2021) employed many sites, including several with higher aerosol loads, yielding thousands of data points with AOD>0.4 at 440 nm, where inversion

525 uncertainties are lower. In contrast, the GAW-PFR network includes fewer stations, mostly under pristine conditions.



Therefore, in the present study it is of particular interest the performance of GRASP under low aerosol loads. Moreover, the availability of parallel observations from both AERONET and GAW-PFR, and the PFR's one-minute temporal resolution, allowed a different validation methodology. Another difference is instrument spectral range: CIMEL covers seven or eight  
530 wavelengths (340-1020 nm or 340-1640 nm), whereas PFR covers four (368-862 nm). A key question was whether the PFR's information content suffices to retrieve SD parameters with similar quality. Our findings show that the PFR's spectral range and resolution are sufficient to retrieve aerosol SD parameters using GRASP—except  $R_{V_c}$ , as also noted by Torres and Fuentes, (2021).

The best GRASP-PFR performance is evident in  $AOD_f$  and  $AOD_c$  retrievals, where we observe the highest correlations and  
535 the lowest (or among the lowest) relative differences against AER-SKY. Most differences between GRASP-PFR and AER-SDA (78% for  $AOD_f$  and 85% for  $AOD_c$ ) lie within AER-SDA uncertainty estimates. AOD modal separation performed excellently for AOD as low as 0.03 at 500 nm across different aerosol types (dust, Sect. 3.3.1; long-range smoke, Sect. 3.3.2). The volume concentrations ( $C_{VT}$ ,  $C_{Vf}$  and  $C_{Vc}$ ) showed good correlations between GRASP-PFR and AER-SKY ( $R > 0.85$ ) with relative median differences of 9-28 %. Relative standard deviations and RMSEs of the linear fit between GRASP-PFR and  
540 AER-SKY, however, ranged 38-55 %.  $C_{Vc}$  from GRASP-PFR was overestimated for predominantly dusty data; this bias disappeared via a carefully selected initial guess of  $R_{Vc}$ .

Volume radii ( $R_{eff}$ ,  $R_{Vf}$ ,  $R_{Vc}$ ) showed variable performance in the comparisons between GRASP-PFR and SKY-AER, depending on the parameter and conditions.  $R_{Vf}$  is a parameter with low variability, which results in a low correlation factor even for small relative differences. It shows the lowest relative standard deviation (22.6%) if we exclude  $AOD_f$  and  $AOD_c$ .  
545 However, only 15% of the differences between GRASP-PFR and AER-SKY were within the AER-SKY uncertainties. Our findings showed that the largest deviations occur at low AE. Restricting the analysis to  $AE > 1$ ,  $AOD > 0.1$  and  $AOD_c > 0.04$  at 500 nm, we showed that there is significant increase in the correlation factor and decrease in the variance of the GRASP-PFR – AER-SKY differences.  $R_{Vc}$  on the other hand does not improve when restricting the data to specific conditions due to its low sensitivity in PFR AOD. For  $R_{Vc}$  only 10% of the differences lie within the AER-SKY uncertainties. However, it can be  
550 improved by providing to GRASP a single  $R_{Vc}$  initial guess close to the average of AER-SKY.  $R_{eff}$  showed a variable performance similar to  $R_{Vf}$  (significant improvement for  $AE > 1$ ,  $AOD > 0.1$  and  $AOD_c > 0.04$ ).  $R_{eff}$  is affected by the performance of  $R_{Vf}$  and  $R_{Vc}$  depending on the concentrations. When the aerosol load is mostly fine particles,  $R_{eff}$  will be affected mostly by the accuracy of  $R_{Vf}$ . When the aerosol load consists of mostly coarse particles, is affected more by the accuracy of  $R_{Vc}$ . As a result, when AE is large enough the more accurate  $R_{Vf}$  and low weight of  $R_{Vc}$  result in a better  $R_{eff}$  estimation. In the opposite  
555 case the accuracy is largely reduced. Conversely, accuracy falls when AE is low, unless the  $R_{Vc}$  initial guess approximates reality.

Regarding the effect of refractive index assumption, we found that using a single value of complex refractive index as input to GRASP showed no significant differences compared to the use of climatologies depending on the month and the station. This was a result of the fixed value being close to the average of the climatologies and showing small enough deviations from them  
560 not to largely affect the statistics of the retrieval comparisons. This is a useful finding for the application of GRASP to GAW-



PFR network since most of the sites do not include a co-located AERONET instrument to provide consistently long-term local observations for the refractive index. In such stations the refractive index selection and the  $R_{Vc}$  initial guess could be a fixed value or climatologies derived from satellite data (Chen et al., 2020), modelling (Taylor et al., 2014), or in-situ ground-based or airborne observations (Espinosa et al., 2017; Espinosa et al., 2019).

565 To assess the effect of wavelength selection on the retrievals of the SD parameters, we used four different AOD datasets corresponding to two different wavelength selections and two AOD calculation methods. One wavelength selection included seven wavelengths similar to CIMEL in the 340-1022 nm range and the second sixteen wavelengths in the 340-2130 nm range. For both wavelength selections we used the observed AOD and the AOD estimated through Eq. (2). Our results showed that the wavelength selection affects the results regardless of the use of the observed AOD or a smooth spectral AOD function  
570 corresponding to the Angström law. The magnitude of the differences varied depending on the compared datasets and the parameter under study. Regarding the wavelength selections, we found that using the larger spectral range,  $R_{Vc}$  is no longer stuck very close to the initial guess (as it happens for the PFR and CIMEL spectral ranges). The additional infrared channels create some sensitivity of  $R_{Vc}$  to the AOD values.

Using AER-SKY retrievals as reference, we found either positive or negative effects when using the larger spectral range in  
575 the aerosol characterization. Most parameters showed small differences in terms of GRASP-BTS and AER-SKY correlation between the different wavelength selections ( $\Delta R < 0.15$  except when comparing  $R_{Vf}$  or  $R_{Vc}$  retrieved from observed AOD to  $R_{Vf}$  retrieved from extrapolated AOD). The relative difference between the medians and the standard deviations of the GRASP-BTS – AER-SKY comparison varies from 0% to 88% depending on the parameter and the datasets compared. We also found no consistent improvement to all properties when using one particular AOD dataset over the retrievals from the other three.  
580 The main positive effect of using a larger spectral range was a reduced standard deviation of the radii differences between GRASP-BTS and AER-SKY compared to the selection of fewer wavelengths. However, this was accompanied by an increased median difference. Possible explanations for this increased bias can be related to the uncertainties of AOD and the GRASP retrievals from AOD or how GRASP responds for the wavelength selection, but in this particular case, for  $R_{eff}$  and  $R_{Vc}$ , the following explanation is probably more important. Using an  $R_{Vc}$  initial guess close to the AER-SKY average and a smaller  
585 spectral range results in GRASP-BTS  $R_{Vc}$  retrievals close to that  $R_{Vc}$  average. If the variability of  $R_{Vc}$  in a particular place or dataset is low and we provide the average to GRASP as an initial guess, then using AOD with the smaller spectral range (seven wavelengths) will result in GRASP remaining close to reality. If instead we use the larger spectral range to retrieve  $R_{Vc}$ , some retrievals will deviate more from the initial guess despite the proximity of the initial guess to reality, as the retrieval retains some uncertainty and the model needs to fit six SD parameters during the inversion. This may result in more accurate  $R_{Vc}$   
590 retrieval when using the smaller spectral range selection compared to the larger. Smaller accuracy in  $R_{Vc}$  retrieval will result in lower accuracy of  $R_{eff}$  retrieval, to some extent may affect  $C_{VT}$ ,  $AOD_c$  and  $C_{Vc}$  as well. However, we used a small number of AERONET measurements that correspond to a station of low aerosol load that corresponds mostly to the fine mode. We also used an initial guess based on the presence of AERONET instrument. This results in more accurate GRASP retrievals when using the selection of seven wavelengths than expected for cases where less information is available or the coarse mode



595 aerosols show larger load and variability. This increased accuracy can ‘hide’ potential benefits of the increased spectral range and our conclusions cannot be generalized. The median  $R_{Vc}$  of AER-SKY in the data used for comparison of Tables 5-6 is  $1.64 \mu\text{m}$ . For GRASP-BTS using AOD at seven wavelengths, the median  $R_{Vc}$  is  $1.78 \mu\text{m}$  and the used initial guess is  $1.75 \mu\text{m}$ . The median GRASP-BTS retrieved  $R_{Vc}$  using AOD at sixteen wavelengths, including  $2130 \text{ nm}$ , is  $1.27 \mu\text{m}$ . Therefore, we can explain the decreased bias of  $R_{Vc}$  compared to AERONET when using seven wavelengths through the proximity between the  
600 AERONET average of this dataset and the initial guess. However, the median of the full GRASP-BTS dataset (81 measurements) using AOD from both wavelength selections is  $1.76 \mu\text{m}$  and the one corresponding to all 81 AER-SKY measurements  $2.55 \mu\text{m}$ . However, 54 of the 81 measurements correspond to  $\text{AOD}_c < 0.02$  at  $500 \text{ nm}$  reducing the significance and the precision of retrieving coarse mode properties. In Fig. 9 (panel c) we can see that  $R_{Vc}$  when using sixteen wavelengths showed a significant portion of low values ( $< 1.3 \mu\text{m}$ ), but the majority of the data corresponds to values closer to the more  
605 usual range of AER-SKY values. We found no clear correlation between  $R_{Vc}$  from GRASP-BTS at sixteen wavelengths and AOD, AE or  $\text{AOD}_c$  except that  $R_{Vc} < 1.4 \mu\text{m}$  rarely appeared for  $\text{AOD}_c > 0.23$  or  $\text{AOD} > 0.26$  at  $500 \text{ nm}$ . Therefore, we cannot attribute the low values and low accuracy of  $R_{Vc}$  from GRASP-BTS using the higher spectral range to the increased  $\text{AOD}_c$  of the retrained measurements compared to the other 54 measurements. The reason of this discrepancy is unclear, but the sample size is particularly small. Comparing the correlation factors between GRASP-BTS and AER-SKY we found improvement  
610 when using the sixteen-wavelength selection ( $R=0.46$  for seven wavelengths of AOD and  $R=0.6$  for sixteen). Using all 81 measurements, we found a larger improvement for R ( $0.06$  when using seven wavelengths and  $0.53$  when using sixteen). Therefore, it is not clear how the conditions affect the GRASP-BTS data accuracy due to the limited data with sufficient coarse mode particles.

The comparison between AER-SKY and GRASP-BTS in most cases shows smaller differences when using the observed AOD  
615 compared to the extrapolated with the same wavelength selection, despite the noise of the observed AOD. This is an indication that cases where reality deviates significantly from the Angström law may result in observable effects on the SD parameter retrievals. Therefore, the observed AOD or a more representative smooth function should be used for this purpose, but still the limited data does not allow high confidence or generalized conclusions.

The GRASP-BTS – AER-SKY comparison showed good consistency in most cases (Tables 2, 5 and 6) with GRASP-PFR –  
620 AER-SKY comparison, although the first corresponds to only a small number of measurements (up to 81) that were not included in the GRASP-PFR and concern only one of the four selected stations. PFR and BTS also show differences between their AOD, which were limited by filtering the BTS AOD using the PFR as reference (Sect. 2.4). Using the AOD-obs dataset at seven wavelengths from BTS, we found the best consistency between the GRASP-PFR and GRASP-BTS comparisons against AER-SKY, which was expected. Most  $\Delta R$  values in that case were below  $0.1$  (higher, up to  $0.2$  for  $R_{Vf}$  and  $C_{Vf}$ ). The  
625 relative differences between the median differences of GRASP-PFR – AER-SKY and GRASP-BTS – AER-SKY, remained below  $9\%$  except for  $C_{VT}$ ,  $C_{Vf}$  and  $R_{\text{eff}}$ , which exceeded  $20\%$ . The st.d. differences were below  $8\%$  except for  $C_{VT}$  and  $C_{Vc}$  that exceeded  $15\%$ , reaching up to  $31\%$ . For the other three BTS AOD datasets there were several cases of larger differences up to  $49\%$ , for  $\Delta$ median and  $\Delta$ st.d. relative differences ( $R_{\text{eff}}$  from sixteen-wavelength AOD dataset) or  $\Delta R < -0.8$  ( $R_{Vf}$  from AOD-



ext), which is a result of the different wavelength selection and AOD calculation method. Retrievals from AOD-obs at sixteen  
630 wavelengths showed reduced s.t.d. of the  $R_{Vc}$  differences with AER-SKY and higher R, which further shows that the additional  
spectral range may improve the retrieval of  $R_{Vc}$ .

In the case of the unusual smoke episode we studied, we found that GRASP can be particularly sensitive to the settings in such  
conditions. Using single retrievals instead of the multi-initial guess approach and more general settings, it was enough to  
reproduce with GRASP the characteristics of this rare aerosol SD using AOD from three different instruments, but with an  
635 underestimation in the concentration and radius of the aerosols. Testing this in one more AERONET station, we found  
consistent results. Using the spectral range and resolution of BTS, we were able to test the effect of wavelength selection in  
this case. The SD did not show sensitivity to the wavelength selections during this smoke episode in Davos.

## 5 Summary and conclusions

In this study, we used the GRASP model to retrieve aerosol SD properties and AOD modal separation from AOD observations  
640 at four locations, which include instruments from both the GAW-PFR and AERONET networks. We used as reference the  
AERONET output parameters (AER-SKY and AER-SDA).

The AOD comparisons between PFR and AERONET AOD (either AER-DIR and AER-SKY) in the four sites showed good  
agreement, with all median differences and standard deviations being  $< 0.01$  (the AOD uncertainty at air mass 1).

Separation of AOD into AOD of fine and coarse mode of GRASP-PFR was the output parameter that showed the best  
645 performance. It showed excellent correlation with both AER-SKY and AER-SDA ( $R > 0.98$ ) (Table 2) the median and standard  
deviation of the differences were within the uncertainties of the AER-SDA retrievals and at least 78% of the points within the  
uncertainties as well.

Volume concentration retrievals showed very good correlation between GRASP-PFR and AER-SKY ( $R \sim 0.88-0.96$ ). The  
relative median differences were above 20% for  $C_{VT}$  and  $C_{Vc}$ , while for  $C_{Vf}$  the median difference was 9%. The relative standard  
650 deviations were above 40% showing larger relative variance in the comparisons compared to the other parameters except  $R_{eff}$ .  
The radii retrievals showed lower correlation ( $R \sim 0.4-0.84$ ) compared to the AOD separation and the concentrations.  $R_{eff}$   
showed overestimation and large variance at larger  $R_{eff}$  values ( $> 0.5-0.7 \mu m$ ) or smaller AE ( $AE < 1-1.3$ ).  $R_{Vf}$  and  $R_{Vc}$  showed  
the lowest correlation and no more than 15% of the GRASP-PFR – AER-SKY differences were within the AER-SKY  
uncertainties.  $R_{Vf}$  has low variability and the correlation factor is not so representative indicator of its performance. It can be  
655 significantly improved by limiting the datasets to observations corresponding to AOD at  $500 \text{ nm} > 0.1$  and  $AE > 1$ . For  $R_{Vc}$   
we found no improvement by limiting the datasets to certain conditions.  $R_{Vc}$  showed improvement when we provided an  $R_{Vc}$   
initial guess closer to the reference median  $R_{Vc}$ . For the radii, no more than 15% of the differences were within the AERONET-  
SKY uncertainties.

Comparing our results with the equivalent ones from Torres and Fuertes, (2021) for GRASP retrieval using AERONET AOD,  
660 we found good consistency between the two studies, despite the differences in the instrument characteristics, site selection and



intercomparison methodology. The results were also not significantly affected by the retrieval under our selections of complex refractive indices, which shows that the aerosol size characterization is possible without the presence of an instrument dedicated to the refractive index observation if the selection is not too far from reality.

Using different wavelength selections from BTS AOD, we found that GRASP-BTS retrievals are affected by the AOD wavelength selection. We also found that  $R_{V_c}$  shows some sensitivity to AOD when we include long enough wavelengths and the correlation factor increases in that case. However, using an  $R_{V_c}$  initial guess close to the average of reality under low variability of  $R_{V_c}$  there may be no benefit to using the larger spectral range. Regarding the other parameters, we found no consistent improvement. The performance was similar to the performance of GRASP-PFR retrievals. Our results correspond to limited AERONET data only on one site with mostly pristine conditions and fine mode aerosols, which limits our capabilities to derive conclusions. Additional sites and more research are required to achieve more solid conclusions regarding the benefit of the larger spectral range in such retrievals. Assessing the differences between the GRASP-PFR and GRASP-BTS comparisons with AER-SKY, further supported the aforementioned conclusions.

Focusing on conditions where the predominant aerosol type is dust, we found consistent results with the findings found above. As dust particles are mainly large enough to correspond in the coarse mode, such cases lead to small AE and large  $R_{\text{eff}}$ , which results in less accurate retrieval of the radii. The results were good as expected for AOD modal separation and volume concentrations. Again,  $R_{\text{eff}}$  and  $R_{V_c}$  showed improvement through the selection of  $R_{V_c}$  initial guess based on  $R_{V_c}$  AER-SKY retrievals.

Finally, in the case of unusual AOD observations during an episode of smoke from the Canadian wildfires in 2023 (negative AE up to 500 nm), we found that the aerosol SD is also unusual. SD included mostly fine mode particles that were unusually large for their type and present in high concentration. GRASP retrievals using AOD from different instruments (PFR, CIMEL and BTS) successfully reproduced these characteristics, but showed overestimation of concentration and radius.

*Code availability.* The GRASP software and documentation is available at the relevant GRASP-SAS website: <https://www.grasp-open.com/>

685

*Data availability.* The PFR AOD data and GRASP-PFR retrievals are available in Zenodo (Karanikolas et al., 2024). The BTS AOD is available in communication with authors.

The CIMEL AOD data are available from <https://aeronet.gsfc.nasa.gov/>. The following references correspond to each site:

Davos: Kouremeti et al., 2024.

690 Hohenpeissenberg: Mattis et al., 2024.

Izaña: Goloub et al., 2024.

Lindenberg: Becker et al., 2024.



695 *Author contribution.* AK analysed the data and wrote the paper with contributions from the co-authors. AK and SK conceptualized the study. BT contributed to the algorithm development and modification for GRASP retrievals from AERONET and GAW-PFR AOD. BT, MM and MHG contributed to the understanding and operation of the GRASP model. MM contributed to the GRASP configuration for retrievals from the BTS spectroradiometer AOD. NK and SK contributed to the PFR sun photometer data provision. JG contributed to the BTS data provision. LD contributed to the PFR sun photometer data provision in Lindenberg. All authors were involved in the interpretation of the results and reviewing the paper.

700 *Competing interests.* The authors declare that they have no conflict of interest.

*Financial support.* This research has been supported by the European Metrology Programme for Innovation and Research (grant no. 19ENV04 MAPP) and COST (European Cooperation in Science and Technology) under the HARMONIA (International network for harmonization of atmospheric aerosol retrievals from ground-based photometers), action no. CA21119.

705

*Acknowledgments.* The authors would like to acknowledge the ESA project QA4EO, grant no. QA4EO/SER/SUB/09 and HARMONIA (International network for harmonization of atmospheric aerosol retrievals from ground-based photometers), action CA21119.

710 Angelos Karanikolas has been supported by the European Metrology Program for Innovation and Research (EMPIR) within the joint research project EMPIR 19ENV04 MAPP “Metrology for aerosol optical properties”. EMPIR is jointly funded by the EMPIR participating countries within EURAMET and the European Union.

Stelios Kazadzis, Angelos Karanikolas and Natalia Kouremeti would like to acknowledge the ACTRIS Switzerland project (Aerosol, Clouds and Trace Gases Research Infrastructure – Swiss contribution) funded by the Swiss State Secretariat for Education, Research and Innovation.

715 Angelos Karanikolas would like to acknowledge Dr. Juan Carlos Antuña Sánchez for the IT support regarding access and operational issues related to the GRASP software.

## References

- Abdillah, S. F. I., You, S. J., Wang, Y.F.: Characterizing Traffic-Related Ultrafine Particles in Roadside Microenvironments: Spatiotemporal Insights from Industrial Parks. *Aerosol Air Qual. Res.* 24, 230295, <https://doi.org/10.4209/aaqr.230295>, 2024.
- 720 Ackerman, K. L., Nugent, A. D., and Taing, C.: Mechanisms controlling giant sea salt aerosol size distributions along a tropical orographic coastline, *Atmos. Chem. Phys.*, 23, 13735–13753, <https://doi.org/10.5194/acp-23-13735-2023>, 2023.



- Alonso-Blanco, E., Calvo, A. I., Pont, V., Mallet, M., Fraile, R., and Castro, A.: Impact of biomass burning on aerosol size distribution, aerosol optical properties and associated radiative forcing, *Aerosol Air Qual. Res.*, 14, 708–724, <https://doi.org/10.4209/aaqr.2013.05.0163>, 2014.
- 725 Andrews, E., Sheridan, P. J., Fiebig, M., McComiskey, A., Ogren, J. A., Arnott, P., Covert, D., Elleman, R., Gasparini, R., Collins, D., Jonsson, H., Schmid, B., and Wang, J.: Comparison of methods for deriving aerosol asymmetry parameter, *J. Geophys. Res.*, 111, D05S04, <https://doi.org/10.1029/2004jd005734>, 2006.
- Bais, A. F., Lucas, R. M., Bornman, J. F., Williamson, C. E., Sulzberger, B., Austin, A. T., Wilson, S. R., Andrady, A. L., Bernhard, G., McKenzie, R. L., Aucamp, P. J., Madronich, S., Neale, R. E., Yazar, S., Young, A. R., de Gruijl, F. R., Norval, M., Takizawa, Y., Barnes, P. W., Robson, T. M., Robinson, S. A., Bailaré, C. L., Flint, S. D., Neale, P. J., Hylander, S., Rose, K. C., Wängberg, S.-Å., Hader, D.-P., Worrest, R. C., Zepp, R. G., Paul, N. D., Cory, R. M., Solomon, K. R., Longstreth, J., Pandey, K. K., Redhwi, H. H., Torikai, A., and Heikkilä, A. M.: Environmental effects of ozone depletion, UV radiation and interactions with climate change: UNEP Environmental Effects Assessment Panel, update 2017, *Photoch. Photobio. Sci.*, 17, 127–179, <https://doi.org/10.1039/c7pp90043k>, 2018.
- 730 Barreto, A., Cuevas, E., Granados-Muñoz, M., Alados-Arboledas, L., Romero, P. M., Gröbner, J., Kouremeti, N., Almansa, A. F., Stone, T., Toledano, C., Román, R., Sorokin, M., Holben, B., Canini, M., and Yela, M.: The new sun-sky-lunar Cimel CE318-T multiband photometer– a comprehensive performance evaluation, *Atmos. Meas. Tech.*, 9, 631–654, <https://doi.org/10.5194/amt-9-631-2016>, 2016.
- Barreto, Á., García, R. D., Guirado-Fuentes, C., Cuevas, E., Almansa, A. F., Milford, C., Toledano, C., Expósito, F. J., Díaz, J. P., and León-Luis, S. F.: Aerosol characterisation in the subtropical eastern North Atlantic region using long-term AERONET measurements, *Atmos. Chem. Phys.*, 22, 11105–11124, <https://doi.org/10.5194/acp-22-11105-2022>, 2022.
- Barnes, P. W., Williamson, C. E., Lucas, R. M., Robinson, S. A., Madronich, S., Paul, N. D., Bornman, J. F., Bais, A. F., Sulzberger, B., Wilson, S. R., Andrady, A. L., McKenzie, R. L., Neale, P. J., Austin, A. T., Bernhard, G. H., Solomon, K. R., Neale, R. E., Young, P. J., Norval, M., Rhodes, L. E., Hylander, S., Rose, K. C., Longstreth, J., Aucamp, P. J., Ballaré, C. L., Cory, R. M., Flint, S. D., de Gruijl, F. R., Häder, D.-P., Heikkilä, A. M., Jansen, M. A. K., Pandey, K. K., Robson, T. M., Sinclair, C. A., Wängberg, S.-Å., Worrest, R. C., Yazar, S., Young, A. R., and Zepp, R. G.: Ozone depletion, ultraviolet radiation, climate change and prospects for a sustainable future, *Nature Sustainability*, 2, 569–579, <https://doi.org/10.1038/s41893-019-0314-2>, 2019.
- 745 Becker, R., Doppler, L., and International AERONET Federation: Lindenberg Aerosol Optical Depth (AOD) with Precipitable Water and Angstrom Parameter level 2.0, Spectral Deconvolution Algorithm (SDA) Retrievals--Fine Mode AOD, Coarse Mode AOD, and Fine Mode Fraction, Volume Size Distribution, Size Distribution Parameters, Extinction AOD, Uncertainty Estimates, Version 3 Direct Sun and Inversion Algorithm, Goddard space flight centre, NASA [data set], [https://aeronet.gsfc.nasa.gov/cgi-bin/webtool\\_aod\\_v3?stage=3&region=Europe&state=Switzerland&site=Davos&place\\_code=10&if\\_polarized=0](https://aeronet.gsfc.nasa.gov/cgi-bin/webtool_aod_v3?stage=3&region=Europe&state=Switzerland&site=Davos&place_code=10&if_polarized=0), last access: 10 March 2024.



- 755 Cachorro, V. E., Berjon, A., Toledano, C., Mogo, S. N., Prats, A. M., De Frutos, J. Vilaplana, M., Vilaplana, J. M., Sorribas, M., De La Morena, B. A., Gröbner, J., Laulainen, N.: Detailed aerosol optical depth intercomparison between Brewer and Li-Cor 1800 spectroradiometers and a Cimel sun photometer, *J. Atmos. Ocean. Tech.*, 26, no. 8: 1558-1571, 2009.
- Correa, L. F., Folini, D., Chtirkova, B. and Wild, M.: Causes for Decadal Trends in Surface Solar Radiation in the Alpine Region in the 1981-2020 Period, *J. Geophys. Res.-Atmos.*, 129(9), <https://doi.org/10.1029/2023JD039998>, 2024.
- 760 Giles, D. M., Sinyuk, A., Sorokin, M. G., Schafer, J. S., Smirnov, A., Slutsker, I., Eck, T. F., Holben, B. N., Lewis, J. R., Campbell, J. R., Welton, E. J., Korkin, S. V., and Lyapustin, A. I.: Advancements in the Aerosol Robotic Network (AERONET) Version 3 database – automated near-real-time quality control algorithm with improved cloud screening for Sun photometer aerosol optical depth (AOD) measurements, *Atmos. Meas. Tech.*, 12, 169–209, <https://doi.org/10.5194/amt-12-169-2019>, 2019.
- 765 Chen, C., Dubovik, O., Fuertes, D., Litvinov, P., Lapyonok, T., Lopatin, A., Ducos, F., Derimian, Y., Herman, M., Tanré, D., Remer, L. A., Lyapustin, A., Sayer, A. M., Levy, R. C., Hsu, N. C., Descloitres, J., Li, L., Torres, B., Karol, Y., Herrera, M., Herreras, M., Aspetsberger, M., Wanzenboeck, M., Bindreiter, L., Marth, D., Hangler, A., and Federspiel, C.: Validation of GRASP algorithm product from POLDER/PARASOL data and assessment of multi-angular polarimetry potential for aerosol monitoring, *Earth Syst. Sci. Data*, 12, 3573–3620, <https://doi.org/10.5194/essd-12-3573-2020>, 2020.
- 770 Cuevas, E., Romero-Campos, P. M., Kouremeti, N., Kazadzis, S., Räisänen, P., García, R. D., Barreto, A., Guirado-Fuentes, C., Ramos, R., Toledano, C., Almansa, F., and Gröbner, J.: Aerosol optical depth comparison between GAW-PFR and AERONET-Cimel radiometers from long-term (2005–2015) 1 min synchronous measurements, *Atmos. Meas. Tech.*, 12, 4309–4337, <https://doi.org/10.5194/amt-12-4309-2019>, 2019.
- Deng, C., Li, Y., Yan, C., Wu, J., Cai, R., Wang, D., Liu, Y., Kangasluoma, J., Kerminen, V.-M., Kulmala, M., and Jiang, J.: Measurement report: Size distributions of urban aerosols down to 1 nm from long-term measurements, *Atmos. Chem. Phys.*, 22, 13569–13580, <https://doi.org/10.5194/acp-22-13569-2022>, 2022.
- Doppler, L., Oehlschlägel, L. M., Miri, R., Tunn, S., and Fischer, J.: The radiation and remote sensing measurements at twin stations Berlin/Lindenberg, a comparison analysis between a suburban and a rural site. In *AIP Conference Proceedings* (Vol. 2988, No. 1). AIP Publishing, [tps://doi.org/10.1063/5.0183679](https://doi.org/10.1063/5.0183679), 2024.
- 780 Dubovik, O. and King, M. D.: A flexible inversion algorithm for retrieval of aerosol optical properties from Sun and sky radiance measurements, *J. Geophys. Res.-Atmos.*, 105, 20673–20696, <https://doi.org/10.1029/2000JD900282>, 2000.
- Dubovik, O., Lapyonok, T., Litvinov, P., Herman, M., Fuertes, D., Ducos, F., Torres, B., Derimian, Y., Huang, X., Lopatin, A., Chaikovsky, A., Aspetsberger, M., and Federspiel, C.: GRASP: a versatile algorithm for characterizing the atmosphere, in: *SPIE, vol. Newsroom*, <https://doi.org/10.1117/2.1201408.005558>, 2014.
- 785 Dubovik, O., Fuertes, D., Litvinov, P., Lopatin, A., Lapyonok, T., Dubovik, I., Xu, F., Ducos, F., Chen, C., Torres, B., Derimian, Y., Li, L., Herreras-Giralda, M., Herrera, M., Karol, Y., Matar, C., Schuster, G. L., Espinosa, R., Puthukkudy, A., Li, Z., Fischer, J., Preusker, R., Cuesta, J., Kreuter, A., Cede, A., Aspetsberger, M., Marth, D., Bindreiter, L., Hangler, A., Lanzinger, V., Holter, C., and Federspiel, C.: A Comprehensive Description of Multi-Term LSM for Applying Multiple a



- Priori Constraints in Problems of Atmospheric Remote Sensing: GRASP Algorithm, Concept, and Applications, *Front. Remote Sens.*, 2, 706851, <https://doi.org/10.3389/frsen.2021.706851>, 2021.
- Eck, T. F., Holben, B. N., Reid, J. S., Sinyuk, A., Giles, D. M., Arola, A., Slutsker, I., Schafer, J. S., Sorokin, M. G., Smirnov, A., LaRosa, A. D., Kraft, J., Reid, E. A., O'Neill, N. T., Welton, E. J., and Menendez, A. R.: The extreme forest fires in California/Oregon in 2020: Aerosol optical and physical properties and comparisons of aged versus fresh smoke, *Atmos. Environ.*, 305, 119798, <https://doi.org/10.1016/j.atmosenv.2023.119798>, 2023.
- Ehlers, K., and Moosmüller, H.: Small and large particle limits of the asymmetry parameter for homogeneous, spherical particles. *Aerosol Science and Technology*, 57(5), 425-433, <https://doi.org/10.1080/02786826.2023.2186214>, 2023.
- Espinosa, W. R., Remer, L. A., Dubovik, O., Ziemba, L., Beyersdorf, A., Orozco, D., Schuster, G., Lapyonok, T., Fuertes, D., and Martins, J. V.: Retrievals of aerosol optical and microphysical properties from Imaging Polar Nephelometer scattering measurements, *Atmos. Meas. Tech.*, 10, 811–824, <https://doi.org/10.5194/amt-10-811-2017>, 2017.
- Espinosa, W. R., Martins, J. V., Remer, L. A., Dubovik, O., Lapyonok, T., Fuertes, D., Puthukkudy, A., Orozco, D., Ziemba, L., Thornhill, K. L., and Levy, R.: Retrievals of Aerosol Size Distribution, Spherical Fraction, and Complex Refractive Index From Airborne In Situ Angular Light Scattering and Absorption Measurements, *J. Geophys. Res.-Atmos.*, 124, 7997–8024, <https://doi.org/10.1029/2018JD030009>, 2019.
- Ezhova, E., Yliviinka, I., Kuusk, J., Komsaare, K., Vana, M., Krasnova, A., Noe, S., Arshinov, M., Belan, B., Park, S.-B., Lavrič, J. V., Heimann, M., Petäjä, T., Vesala, T., Mammarella, I., Kolari, P., Bäck, J., Rannik, Ü., Kerminen, V.-M., and Kulmala, M.: Direct effect of aerosols on solar radiation and gross primary production in boreal and hemiboreal forests, *Atmos. Chem. Phys.*, 18, 17863–17881, <https://doi.org/10.5194/acp-18-17863-2018>, 2018.
- Fountoulakis, I., Natsis, A., Siomos, N., Drosoglou, T., and Bais, F. A.: Deriving Aerosol Absorption Properties from Solar Ultraviolet Radiation Spectral Measurements at Thessaloniki, Greece, *Remote Sens.*, 11, 2179, <https://doi.org/10.3390/rs11182179>, 2019.
- Giles, D. M., Sinyuk, A., Sorokin, M. G., Schafer, J. S., Smirnov, A., Slutsker, I., Eck, T. F., Holben, B. N., Lewis, J. R., Campbell, J. R., Welton, E. J., Korkin, S. V., and Lyapustin, A. I.: Advancements in the Aerosol Robotic Network (AERONET) Version 3 database – automated near-real-time quality control algorithm with improved cloud screening for Sun photometer aerosol optical depth (AOD) measurements, *Atmos. Meas. Tech.*, 12, 169–209, <https://doi.org/10.5194/amt-12-169-2019>, 2019.
- Glotfelty, T., Alapaty, K., He, J., Hawbecker, P., Song, X., and Zhang, G.: The Weather Research and Forecasting Model with Aerosol-Cloud Interactions (WRF-ACI): Development, Evaluation, and Initial Application, *Mon. Weather Rev.*, 147, 1491–1511, <https://doi.org/10.1175/MWR-D-18-0267.1>, 2019.
- Goessling, H. F., Rackow, T., and Jung, T.: Recent global temperature surge intensified by record-low planetary albedo, *Science*, eadq7280, 10.1126/science.adq7280, 2024.
- Goloub, P., Damiri, B., Cuevas, E., Barreto, A., and International AERONET Federation: Izaña Aerosol Optical Depth (AOD) with Precipitable Water and Angstrom Parameter level 2.0, Spectral Deconvolution Algorithm (SDA) Retrievals--Fine Mode



- AOD, Coarse Mode AOD, and Fine Mode Fraction, Volume Size Distribution, Size Distribution Parameters, Extinction AOD, Uncertainty Estimates, Version 3 Direct Sun and Inversion Algorithm, Goddard space flight centre, NASA [data set],  
825 [https://aeronet.gsfc.nasa.gov/cgi-bin/webtool\\_aod\\_v3?stage=3&region=Europe&state=Switzerland&site=Davos&place\\_code=10&if\\_polarized=0](https://aeronet.gsfc.nasa.gov/cgi-bin/webtool_aod_v3?stage=3&region=Europe&state=Switzerland&site=Davos&place_code=10&if_polarized=0), last access: 10 March 2024.
- Gong, S. L., Barrie, L. A., Blanchet, J. P., von Salzen, K., Lohmann, U., Lesins, G., Spacek, L., Zhang, L. M., Girard, E., Lin, H., Leaitch, R., Leighton, H., Chylek, P., and Huang, P.: Canadian Aerosol Module: A size-segregated simulation of atmospheric aerosol processes for climate and air quality models 1. Module development, *J. Geophys. Res.*, 108, 4007,  
830 <https://doi.org/10.1029/2001JD002002>, 2003.
- Gröbner, J., Kouremeti, N., Hülsen, G., Zuber, R., Ribnitzky, M., Nevas, S., Sperfeld, P., Schwind, K., Schneider, P., Kazadzis, S., Barreto, Á., Gardiner, T., Mottungan, K., Medland, D., and Coleman, M.: Spectral aerosol optical depth from SI-traceable spectral solar irradiance measurements, *Atmos. Meas. Tech.*, 16, 4667–4680, <https://doi.org/10.5194/amt-16-4667-2023>, 2023.
- Hernández Pardo, L., Toledo Machado, L. A., Amore Cecchini, M., and Sánchez Gácita, M.: Quantifying the aerosol effect  
835 on droplet size distribution at cloud top, *Atmos. Chem. Phys.*, 19, 7839–7857, <https://doi.org/10.5194/acp-19-7839-2019>, 2019.
- Hodnebrog, Ø., Myhre, G., Jouan, C., Andrews, T., Forster, P. M., Jia, H., Loeb, N. G., Oliví, D. J. L., Paynter, D., Quaas, J., Raghuraman, S. P., and Schulz, M.: Recent reductions in aerosol emissions have increased Earth's energy imbalance, *Commun. Earth Environ.*, 5, 166, <https://doi.org/10.1038/s43247-024-01324-8>, 2024.
- 840 Holben, B. N., Eck, T. F., Slutsker, I., Tanré, D., Buis, J. P., Setzer, A., Vermote, E., Reagan, J. A., Kaufman, Y. J., Nakajima, T., Lavenu, F., Jankowiak, I., and Smirnov, A.: AERONET—A Federated Instrument Network and Data Archive for Aerosol Characterization, *Remote Sens. Environ.*, 66, 1–16, [https://doi.org/10.1016/S0034-4257\(98\)00031-5](https://doi.org/10.1016/S0034-4257(98)00031-5), 1998.
- Holben, B. N., Eck, T. F., Slutsker, I., Smirnov, A., Sinyuk, A., Schafer, J., Giles, D., and Dubovik, O.: Aeronet's Version 2.0 quality assurance criteria, *Proc. SPIE*, 6408, 64080Q, <https://doi.org/10.1117/12.706524>, 2006.
- 845 Horneck, G.: Quantification of the biological effectiveness of environmental UV radiation, *J. Photoch. Photobio. B*, 31, 43–49, [https://doi.org/10.1016/1011-1344\(95\)07167-3](https://doi.org/10.1016/1011-1344(95)07167-3), 1995.
- Hou, X., Papachristopoulou, K., Saint-Drenan, Y.-M., and Kazadzis, S.: Solar Radiation Nowcasting Using a Markov Chain Multi-Model Approach, *Energies*, 15, 2996, <https://doi.org/10.3390/en15092996>, 2022.
- IPCC: Climate Change 2023: Synthesis Report. Contribution of Working Groups I, II and III to the Sixth Assessment Report  
850 of the Intergovernmental Panel on Climate Change [Core Writing Team, Lee, H. and Romero, J. (eds.)]. IPCC, Geneva, Switzerland, 184 pp., doi: 10.59327/IPCC/AR6-9789291691647, 2023.
- Huang, X. and Ding, A.: Aerosol as a critical factor causing forecast biases of air temperature in global numerical weather prediction models, *Sci. Bull.*, 66, 1917–1924, <https://doi.org/10.1016/j.scib.2021.05.009>, 2021.
- Jain, P., Barber, Q.E., Taylor, S.W., Whitman, E., Castellanos Acuna, D., Boulanger, Y., Chavardès, R.D., Chen, J., Englefield,  
855 P., Flannigan, M. and Girardin, M.P.: Drivers and impacts of the record-breaking 2023 wildfire season in Canada, *Nature Communications*, 15(1), 6764, <https://doi.org/10.1038/s41467-024-51154-7>, 2024.



- Karanikolas, A., Kouremeti, N., Gröbner, J., Egli, L., and Kazadzis, S.: Sensitivity of aerosol optical depth trends using long-term measurements of different sun photometers, *Atmos. Meas. Tech.*, 15, 5667–5680, <https://doi.org/10.5194/amt-15-5667-2022>, 2022.
- 860 Karanikolas, A. Datasets of Aerosol properties retrieved from AOD time series at selected GAWPFR stations, Zenodo [Data set], <https://doi.org/10.5281/zenodo.13624808>, 2024.
- Kazadzis, S., Bais, A., Amiridis, V., Balis, D., Meleti, C., Kouremeti, N., Zerefos, C. S., Rapsomanikis, S., Petrakakis, M., Kelesis, A., Tzoumaka, P., and Kelektoglou, K.: Nine years of UV aerosol optical depth measurements at Thessaloniki, Greece, *Atmos. Chem. Phys.*, 7, 2091–2101, <https://doi.org/10.5194/acp-7-2091-2007>, 2007.
- 865 Kazadzis, S., Veselovskii, I., Amiridis, V., Gröbner, J., Suvorina, A., Nyeki, S., Gerasopoulos, E., Kouremeti, N., Taylor, M., Tsekeri, A., and Wehrli, C.: Aerosol microphysical retrievals from precision filter radiometer direct solar radiation measurements and comparison with AERONET, *Atmos. Meas. Tech.*, 7, 2013–2025, <https://doi.org/10.5194/amt-7-2013-2014>, 2014
- Kazadzis, S., Kouremeti, N., Diémoz, H., Gröbner, J., Forgan, B. W., Campanelli, M., Estellés, V., Lantz, K., Michalsky, J., 870 Carlund, T., Cuevas, E., Toledano, C., Becker, R., Nyeki, S., Kosmopoulos, P. G., Tatsiankou, V., Vuilleumier, L., Denn, F. M., Ohkawara, N., Ijima, O., Goloub, P., Raptis, P. I., Milner, M., Behrens, K., Barreto, A., Martucci, G., Hall, E., Wendell, J., Fabbri, B. E., and Wehrli, C.: Results from the Fourth WMO Filter Radiometer Comparison for aerosol optical depth measurements, *Atmos. Chem. Phys.*, 18, 3185–3201, <https://doi.org/10.5194/acp-18-3185-2018>, 2018a.
- Kazadzis, S., Kouremeti, N., Nyeki, S., Gröbner, J., and Wehrli, C.: The World Optical Depth Research and Calibration Center 875 (WORCC) quality assurance and quality control of GAW-PFR AOD measurements, *Geosci. Instrum. Meth.*, 7, 39–53, <https://doi.org/10.5194/gi-7-39-2018>, 2018b.
- Kazadzis, S., Kouremeti, N., and Gröbner, J.: Fifth WMO Filter Radiometer Comparison (FRC-V) 27 September to 25 October 2021, Davos, Switzerland, WMO GAW report 280, <https://library.wmo.int/records/item/66263-fifth-wmo-filter-radiometer-comparison-frc-v?offset=5>, (last access: 1 February 2024), 2023.
- 880 King, M. D., Byrne, D. M., Herman, B. M., and Reagan, J. A.: Aerosol size distributions obtained by the inversion of spectral optical depth measurements, *J. Atmos. Sci.*, 35, 2153–2167, [https://doi.org/10.1175/1520-0469\(1978\)035<2153:ASDOBI>2.0.CO;2](https://doi.org/10.1175/1520-0469(1978)035<2153:ASDOBI>2.0.CO;2), 1978.
- King, M. D.: Sensitivity of constrained linear inversions to the selection of the Lagrange multiplier. *Journal of Atmospheric Sciences*, 39(6), 1356–1369, [https://doi.org/10.1175/1520-0469\(1982\)039<1356:SOCLIT>2.0.CO;2](https://doi.org/10.1175/1520-0469(1982)039<1356:SOCLIT>2.0.CO;2), 1982.
- 885 Kodros, J. K. and Pierce, J. R.: Important global and regional differences in aerosol cloud-albedo effect estimates between simulations with and without prognostic aerosol microphysics, *J. Geophys. Res.*, 122, 4003–4018, <https://doi.org/10.1002/2016JD025886>, 2017.
- Kodros, J. K., Volckens, J., Jathar, S. H., and Pierce, J. R.: Ambient particulate matter size distributions drive regional and global variability in particle deposition in the respiratory tract, *Geohealth*, 2, 298–312, <https://doi.org/10.1029/2018gh000145>, 890 2018.



- Konsta, D., Tsekeri, A., Solomos, S., Siomos, N., Gialitaki, A., Tetoni, E., Lopatin, A., Goloub, P., Dubovik, O., Amiridis, V. and Nastos, P.: The potential of GRASP/GARRLiC retrievals for dust aerosol model evaluation: Case study during the preTECT campaign. *Remote Sensing*, 13(5), p.873, <https://doi.org/10.3390/rs13050873>, 2021.
- 895 Kouremeti, N., Wehrli, C., and International AERONET Federation: Davos Aerosol Optical Depth (AOD) with Precipitable Water and Angstrom Parameter level 2.0, Spectral Deconvolution Algorithm (SDA) Retrievals--Fine Mode AOD, Coarse Mode AOD, and Fine Mode Fraction, Volume Size Distribution, Size Distribution Parameters, Extinction AOD, Uncertainty Estimates, Version 3 Direct Sun and Inversion Algorithm, Goddard space flight centre, NASA [data set], [https://aeronet.gsfc.nasa.gov/cgi-bin/webtool\\_aod\\_v3?stage=3&region=Europe&state=Switzerland&site=Davos&place\\_code=10&if\\_polarized=0](https://aeronet.gsfc.nasa.gov/cgi-bin/webtool_aod_v3?stage=3&region=Europe&state=Switzerland&site=Davos&place_code=10&if_polarized=0), last access: 10 March 2024.
- 900 Levin, Z., Teller, A., Ganor, E., Graham, B., Andreae M. O., Maenhaut W., Falkovich A. H., Rudich Y.: Role of aerosol size and composition in nucleation scavenging within clouds in a shallow cold front, *J. Geophys. Res. Atmos.*, 108, <https://doi.org/10.1029/2003JD003647>, 2003.
- Li, J., Carlson, B. E., Yung, Y. L., Lv, D., Hansen, J., Penner, J. E., Liao, H., Ramaswamy, V., Kahn, R. A., Zhang, P., Dubovik, O., Ding, A., Laci, A. A., Zhang, L., and Dong, Y.: Scattering and absorbing aerosols in the climate system, *Nature Reviews Earth & Environment*, 3, 363–379, <https://doi.org/10.1038/s43017-022-00296-7>, 2022.
- 905 Li, H., Zhang, M., Wang, L., Lu, Y., Yu, L., Ma, Y., Gong, W.: Effects of aerosol on downward diffuse radiation under blowing dust and haze conditions, *Atmospheric Environment*, 334, 120682, <https://doi.org/10.1016/j.atmosenv.2024.120682>, 2024.
- Liu, J.; Li, M.; Zhou, L.; Ge, J.; Liu, J.; Guo, Z.; Liu, Y.; Wang, J.; Yan, Q.; Hua, D. Analysis of Aerosol Optical Depth and Forward Scattering in an Ultraviolet Band Based on Sky Radiometer Measurements. *Remote Sens.*, 15, 4342. <https://doi.org/10.3390/rs15174342>, 2023.
- 910 Maloney, C., Toon, B., Bardeen, C., Yu, P., Froyd, K., Kay, J., and Woods, S.: The Balance Between Heterogeneous and Homogeneous Nucleation of Ice Clouds Using CAM5/CARMA, *J. Geophys. Res.-Atmos.*, 127, e2021JD035540, <https://doi.org/10.1029/2021JD035540>, 2022.
- Mampage, C. B. A., Hughes, D. D., Jones, L. M., Metwali, N., Thorne, P. S., Stone, E. A.: Characterization of sub-pollen particles in size-resolved atmospheric aerosol using chemical tracers, *Atmospheric Environment: X*, 15, 100177, 2590-1621, <https://doi.org/10.1016/j.aeaoa.2022.100177>, 2022.
- 915 Martin, R., Mather, T., Pyle, D., Power, M., Allen, A., Aiuppa, A., Horwell, C., and Ward, E.: Composition-resolved size distributions of volcanic aerosols in the Mt. Etna plumes, *J. Geophys. Res.*, 113, D17211, doi:10.1029/2007JD009648, 2008.
- Maser, M. S. , Jaenicke, R.: The size distribution of primary biological aerosol particles with radii > 0.2  $\mu\text{m}$  in an urban/rural influenced region, *Atmospheric Research*, 39(4), 279-286, [https://doi.org/10.1016/0169-8095\(95\)00017-8](https://doi.org/10.1016/0169-8095(95)00017-8), 1995.
- 920 Mattis, I., and International AERONET Federation: Hohenpeissenberg Aerosol Optical Depth (AOD) with Precipitable Water and Angstrom Parameter level 2.0, Spectral Deconvolution Algorithm (SDA) Retrievals--Fine Mode AOD, Coarse Mode AOD, and Fine Mode Fraction, Volume Size Distribution, Size Distribution Parameters, Extinction AOD, Uncertainty Estimates, Version 3 Direct Sun and Inversion Algorithm, Goddard space flight centre, NASA [data set],



- 925 [https://aeronet.gsfc.nasa.gov/cgi-bin/webtool\\_aod\\_v3?stage=3&region=Europe&state=Switzerland&site=Davos&place\\_code=10&if\\_polarized=0](https://aeronet.gsfc.nasa.gov/cgi-bin/webtool_aod_v3?stage=3&region=Europe&state=Switzerland&site=Davos&place_code=10&if_polarized=0), last access: 10 March 2024.
- Masoom, A., Fountoulakis, I., Kazadzis, S., Raptis, I.-P., Kampouri, A., Psiloglou, B. E., Kouklaki, D., Papachristopoulou, K., Marinou, E., Solomos, S., Gialitaki, A., Founda, D., Salamalikis, V., Kaskaoutis, D., Kouremeti, N., Mihalopoulos, N., Amiridis, V., Kazantzidis, A., Papayannis, A., Zerefos, C. S., and Eleftheratos, K.: Investigation of the effects of the Greek  
930 extreme wildfires of August 2021 on air quality and spectral solar irradiance, *Atmos. Chem. Phys.*, 23, 8487–8514, <https://doi.org/10.5194/acp-23-8487-2023>, 2023.
- Mazzola, M., Stone, R.S., Herber, A., Tomasi, C., Lupi, A., Vitale V., Lanconelli, C., Toledano, C., Cachorro V.E., O'Neill, N.T., Shiobara, M., Aaltonen, V., Stebel, K., Zielinski, T., Petelski, T., Ortiz de Galisteo, J.P., Torres, B., Berjon, A., Goloub, P., Li, Z., Blarel, L., Abboud, I., Cuevas, E., Stock, M., Schulz, K., H., Virkkul, A.; Evaluation of sun photometer capabilities  
935 for retrievals of aerosol optical depth at high latitudes: The POLAR-AOD intercomparison campaigns, *Atmos. Environ.*, 52, 4-17, 2012.
- Mona, L., Papagiannopoulos, N., Basart, S., Baldasano, J., Binietoglou, I., Cornacchia, C., and Pappalardo, G.: EARLINET dust observations vs. BSC-DREAM8b modeled profiles: 12-year-long systematic comparison at Potenza, Italy, *Atmos. Chem. Phys.*, 14, 8781–8793, <https://doi.org/10.5194/acp-14-8781-2014>, 2014.
- 940 Monteiro, A., Basart, S., Kazadzis, S., Votsis, A., Gkikas, A., Vandenbussche, S., Tobias, A., Gama, C., Pérez García-Pando, C., Terradellas, E., Notas, G., Middleton, N., Kushta, J., Amiridis, V., Lagouvardos, K., Kosmopoulos, P., Kotroni, V., Kanakidou, M., Mihalopoulos, N., Kalivitis, N., Dagsson-Waldhauserová, P., El-Askary, H., Sievers, K., Giannaros, T., Mona, L., Hirtl, M., Skomorowski, P., Virtanen, T. H., Christoudias, T., Di Mauro, B., Trippetta, S., Kutuzov, S., Meinander, O., and Nickovic, S.: Multi-sectoral impact assessment of an extreme African dust episode in the Eastern Mediterranean in March  
945 2018, *Sci. Total Environ.*, 843, 156861, <https://doi.org/10.1016/j.scitotenv.2022.156861>, 2022.
- Nakajima, T., Campanelli, M., Che, H., Estellés, V., Irie, H., Kim, S.-W., Kim, J., Liu, D., Nishizawa, T., Pandithurai, G., Soni, V. K., Thana, B., Tugjurn, N.-U., Aoki, K., Go, S., Hashimoto, M., Higurashi, A., Kazadzis, S., Khatri, P., Kouremeti, N., Kudo, R., Marengo, F., Momoi, M., Ningombam, S. S., Ryder, C. L., Uchiyama, A., and Yamazaki, A.: An overview of and issues with sky radiometer technology and SKYNET, *Atmos. Meas. Tech.*, 13, 4195–4218, <https://doi.org/10.5194/amt-13-4195-2020>, 2020.
- 950 Nicolae, V., Talianu, C., Andrei, S., Antonescu, B., Ene, D., Nicolae, D., Dandocsi, A., Toader, V. E., Stefan, S., Savu, T., and Vasilescu, J.: Multiyear typology of long-range transported aerosols over Europe, *Atmosphere*, 10, 482, <https://doi.org/10.3390/atmos10090482>, 2019.
- Nyeki, S., Halios, C. H., Baum, W., Eleftheriadis, K., Flentje, H., Gröbner, J., Vuilleumier, L., and Wehrli, C.: Ground-based aerosol optical depth trends at three high-altitude sites in Switzerland and southern Germany from 1995 to 2010, *Geophys. Res.-Atmos.*, 117, D18202, <https://doi.org/10.1029/2012jd017493>, 2012.
- O'Neill, N. T., Eck, T. F., Smirnov, A., Holben, B. N., and Thulasiraman, S.: Spectral discrimination of coarse and fine mode optical depth, *J. Geophys. Res.-Atmos.*, 108, AAC-8-1–AAC-8-15, <https://doi.org/10.1029/2002JD002975>, 2003.



- Pandolfi, M., Alados-Arboledas, L., Alastuey, A., Andrade, M., Angelov, C., Artiñano, B., Backman, J., Baltensperger, U.,  
960 Bonasoni, P., Bukowiecki, N., Collaud Coen, M., Conil, S., Coz, E., Crenn, V., Dudoitis, V., Ealo, M., Eleftheriadis, K., Favez,  
O., Fetfatzis, P., Fiebig, M., Flentje, H., Ginot, P., Gysel, M., Henzing, B., Hoffer, A., Holubova Smejkalova, A., Kalapov, I.,  
Kalivitis, N., Kouvarakis, G., Kristensson, A., Kulmala, M., Lihavainen, H., Lunder, C., Luoma, K., Lyamani, H., Marinoni,  
A., Mihalopoulos, N., Moerman, M., Nicolas, J., O'Dowd, C., Petäjä, T., Petit, J.-E., Pichon, J. M., Prokopciuk, N., Putaud, J.-  
P., Rodríguez, S., Sciare, J., Sellegri, K., Swietlicki, E., Titos, G., Tuch, T., Tunved, P., Ulevicius, V., Vaishya, A., Vana, M.,  
965 Virkkula, A., Vratolis, S., Weingartner, E., Wiedensohler, A., and Laj, P.: A European aerosol phenomenology – 6: scattering  
properties of atmospheric aerosol particles from 28 ACTRIS sites, *Atmos. Chem. Phys.*, 18, 7877–7911,  
<https://doi.org/10.5194/acp-18-7877-2018>, 2018.
- Papachristopoulou, K., Fountoulakis, I., Bais, A. F., Psiloglou, B. E., Papadimitriou, N., Raptis, I.-P., Kazantzidis, A., Kontoes,  
C., Hatzaki, M., and Kazadzis, S.: Effects of clouds and aerosols on downwelling surface solar irradiance nowcasting and sort-  
970 term forecasting, *Atmos. Meas. Tech. Discussions*, 1–31, <https://doi.org/10.5194/amt-2023-110>, 2023.
- Pérez-Ramírez, D., Veselovskii, I., Whiteman, D. N., Suvorina, A., Korenskiy, M., Kolgotin, A., Holben, B., Dubovik, O.,  
Siniuk, A., and Alados-Arboledas, L.: High temporal resolution estimates of columnar aerosol microphysical parameters from  
spectrum of aerosol optical depth by linear estimation: application to long-term AERONET and star-photometry  
measurements, *Atmos. Meas. Tech.*, 8, 3117–3133, <https://doi.org/10.5194/amt-8-3117-2015>, 2015.
- 975 Rodríguez-Arias, R.M., Rojo J., Fernández-González, F., Pérez-Badia R.: Desert dust intrusions and their incidence on  
airborne biological content. Review and case study in the Iberian Peninsula, *Environmental Pollution*, 316(1), 120464, 0269-  
7491, <https://doi.org/10.1016/j.envpol.2022.120464>, 2023.
- Rosenfeld, D., Sherwood, S., Wood, R., and Donner, L.: Climate Effects of Aerosol-Cloud Interactions, *Science*, 343, 379–  
380, <https://doi.org/10.1126/science.1247490>, 2014.
- 980 Schuster, G. L., Dubovik, O., and Holben, B. N.: Ångström exponent and bimodal aerosol size distributions, *J. Geophys. Res.-  
Atmos.*, 111, D07207, <https://doi.org/10.1029/2005JD006328>, 2006.
- Shao, Y., Zhang, J., Ishizuka, M., Mikami, M., Leys, J., and Huang, N.: Dependency of particle size distribution at dust  
emission on friction velocity and atmospheric boundary-layer stability, *Atmos. Chem. Phys.*, 20, 12939–12953,  
<https://doi.org/10.5194/acp-20-12939-2020>, 2020.
- 985 Shaw, G. E., Reagan, J. A., and Herman, B. M.: Investigations of Atmospheric Extinction Using Direct Solar Radiation  
Measurements Made with a Multiple Wavelength Radiometer, *J. Appl. Meteorol. Clim.*, 12, 374–380,  
[https://doi.org/10.1175/1520-0450\(1973\)012<0374:IOAEUD>2.0.CO;2](https://doi.org/10.1175/1520-0450(1973)012<0374:IOAEUD>2.0.CO;2), 1973.
- Shaw, G. E.: Sun photometry, *Bull. Am. Meteorol. Soc.*, 64, 4–10, 1983.
- Schuster, G. L., Dubovik, O., and Holben, B. N.: Ångström exponent and bimodal aerosol size distributions, *J. Geophys. Res.-  
990 Atmos.*, 111, D07207, <https://doi.org/10.1029/2005JD006328>, 2006.
- Shi S., Cheng T., Gu X., Guo H., Wu Y., Wang Y.: Biomass burning aerosol characteristics for different vegetation types in  
different aging periods, *Environment International*, 126, 504-511, <https://doi.org/10.1016/j.envint.2019.02.073>, 2019.



- Sinyuk, A., Holben, B. N., Eck, T. F., Giles, D. M., Slutsker, I., Korokin, S., Schafer, J. S., Smirnov, A., Sorokin, M., and Lyapustin, A.: The AERONET Version 3 aerosol retrieval algorithm, associated uncertainties and comparisons to Version 2, 995 *Atmos. Meas. Tech.*, 13, 3375–3411, <https://doi.org/10.5194/amt-13-3375-2020>, 2020.
- Smirnov, A., Holben, B., N., Eck, T., F., Dubovik, O., Slutsker, I.: Cloud-screening and quality control algorithms for the AERONET database, *Remote Sens. Environ.*, 73.3, 337-349, 2000.
- Svenningsson B., Hansson H. C., Martinsson B., Wiedensohler A., Swietlicki E., Cederfelt S. I., Wendisch M., Bower K. N., Choularton T. W. , Colvile R. N.: Cloud droplet nucleation scavenging in relation to the size and hygroscopic behaviour of 1000 aerosol particles, *Atmospheric Environment*, 31(16), 2463-2475, [https://doi.org/10.1016/S1352-2310\(96\)00179-3](https://doi.org/10.1016/S1352-2310(96)00179-3), 1997.
- Taylor, M., Kazadzis, S., and Gerasopoulos, E.: Multi-modal analysis of aerosol robotic network size distributions for remote sensing applications: dominant aerosol type cases, *Atmos. Meas. Tech.*, 7, 839–858, <https://doi.org/10.5194/amt-7-839-2014>, 2014.
- Tian, P., Zeren Y., Chen C., Jianping H., Chenliang K., Jinsen S., Xianjie C., and Lei Z.: Atmospheric aerosol size distribution 1005 impacts radiative effects over the Himalayas via modulating aerosol single-scattering albedo, *npj Climate and Atmospheric Science*, 6(1), 54, <https://doi.org/10.1038/s41612-023-00368-5>, 2023.
- Tiwari, M., Sahu, S. K., Bhangare, R. C., Yousaf, A., Pandit, G. G.: Particle size distributions of ultrafine combustion aerosols generated from household fuels, *Atmospheric Pollution Research*, 5, 1, 145-150, <https://doi.org/10.5094/APR.2014.018>, 2014.
- Toledano, C., González, R., Fuertes, D., Cuevas, E., Eck, T. F., Kazadzis, S., Kouremeti, N., Gröbner, J., Goloub, P., Blarel, 1010 L., Román, R., Barreto, Á., Berjón, A., Holben, B. N., and Cachorro, V. E.: Assessment of Sun photometer Langley calibration at the high-elevation sites Mauna Loa and Izaña, *Atmos. Chem. Phys.*, 18, 14555–14567, <https://doi.org/10.5194/acp-18-14555-2018>, 2018.
- Torres, B., Dubovik, O., Fuertes, D., Schuster, G., Cachorro, V. E., Lapyonok, T., Goloub, P., Blarel, L., Barreto, A., Mallet, M., Toledano, C., and Tanré, D.: Advanced characterisation of aerosol size properties from measurements of spectral optical 1015 depth using the GRASP algorithm, *Atmos. Meas. Tech.*, 10, 3743–3781, <https://doi.org/10.5194/amt-10-3743-2017>, 2017.
- Torres, B. and Fuertes, D.: Characterization of aerosol size properties from measurements of spectral optical depth: a global validation of the GRASP-AOD code using long-term AERONET data, *Atmos. Meas. Tech.*, 14, 4471–4506, <https://doi.org/10.5194/amt-14-4471-2021>, 2021.
- Van de Hulst, H.: *Light Scattering by Small Particles*, Structure of Matter Series, John Wiley & Sons, 1957.
- Veselovskii, I., Dubovik, O., Kolgotin, A., Korenskiy, M., Whiteman, D. N., Allakhverdiev, K., and Huseyinoglu, F.: Linear 1020 estimation of particle bulk parameters from multi-wavelength lidar measurements, *Atmos. Meas. Tech.*, 5, 1135–1145, <https://doi.org/10.5194/amt-5-1135-2012>, 2012.
- Virtanen, A., Joutsensaari, J., Kokkola, H., Partridge, D. G., Blichner, S., Seland, Ø., Holopainen, E, Tovazzi, E., Lipponen, A., Mikkonen, S., Leskinen, A.: High sensitivity of cloud formation to aerosol changes. *Nature Geoscience*, 1-7, 1025 [10.1038/s41561-025-01662-y](https://doi.org/10.1038/s41561-025-01662-y), 2025.



- Wehrli, C.: Calibrations of filter radiometers for determination of atmospheric optical depth, *Metrologia*, 37, 419, <https://doi.org/10.1088/0026-1394/37/5/16>, 2000.
- Wehrli, C., Kouremeti, N., and International AERONET Federation: Davos Aerosol Optical Depth (AOD) with Precipitable Water and Angstrom Parameter level 2.0 Version 3 Direct Sun Algorithm, Goddard space flight centre, NASA [data set], [https://aeronet.gsfc.nasa.gov/cgi-bin/webtool\\_aod\\_v3?stage=3&region=Europe&state=Switzerland&site=Davos&place\\_code=10&if\\_polarized=0](https://aeronet.gsfc.nasa.gov/cgi-bin/webtool_aod_v3?stage=3&region=Europe&state=Switzerland&site=Davos&place_code=10&if_polarized=0), last access: 10 March 2024.
- Wild, M.: Enlightening Global Dimming and Brightening, *B. Am. Meteorol. Soc.*, 93, 27–37, <https://doi.org/10.1175/BAMS-D-11-00074.1>, 2012.
- Wild, M., Wacker, S., Yang, S., and Sanchez-Lorenzo, A.: Evidence for Clear-sky Dimming and Brightening in Central Europe, *Geophys. Res. Lett.*, 48, e2020GL092216, <https://doi.org/10.1029/2020GL092216>, 2021.
- Winkler, P. M. and Wagner, P. E.: Characterization techniques for heterogeneous nucleation from the gas phase, *J. Aerosol. Sci.*, 159, 105875, <https://doi.org/10.1016/j.jaerosci.2021.105875>, 2022.
- Weller, M. and Gericke K.: Long-term observations of aerosol optical depths at the Meteorological Observatory Lindenberg, *Meteorologische Zeitschrift (Berlin)* 14, 10.1127/0941-2948/2005/0070, 2005.
- WMO: Aerosol measurement procedures, guidelines and recommendations, GAW Report 153, WMO/TD-No 1178, [https://library.wmo.int/opac/index.php?lvl=notice\\_display&id=11085#.WpqIOOdG1PY](https://library.wmo.int/opac/index.php?lvl=notice_display&id=11085#.WpqIOOdG1PY) (last access: 4 October 2022), 2003.
- Wacker, S., Becker, R., Filipitsch, F., and Doppler, L.: Radiation measurements at the WMO/CIMO testbed site Lindenberg. In *AIP Conference Proceedings* (Vol. 2988, No. 1). AIP Publishing, <https://doi.org/10.1063/5.0183573>, 2024.
- Wendish, M. and von Hoyningen-Huene, W.: Possibility of refractive index determination of atmospheric aerosol particles by ground-based solar extinction and scattering measurements, *Atmospheric Environment*, 28, 784–792, [https://doi.org/10.1016/1352-2310\(94\)90237-2](https://doi.org/10.1016/1352-2310(94)90237-2), 1994.
- Witriol, N. M., Sindoni, O. I., Forward scattering and size parameter in layered spherical aerosol particles, *Journal of Aerosol Science*, 23(1), 349–352, [https://doi.org/10.1016/0021-8502\(92\)90421-Q](https://doi.org/10.1016/0021-8502(92)90421-Q), 1992.
- Wrana, F., Niemeier, U., Thomason, L. W., Wallis, S., and von Savigny, C.: Stratospheric aerosol size reduction after volcanic eruptions, *Atmos. Chem. Phys.*, 23, 9725–9743, <https://doi.org/10.5194/acp-23-9725-2023>, 2023.
- Wu, T. and Boor, B. E.: Urban aerosol size distributions: a global perspective, *Atmos. Chem. Phys.*, 21, 8883–8914, <https://doi.org/10.5194/acp-21-8883-2021>, 2021.
- Xia, X., Chen, H., Li, Z., Wang, P., and Wang, J.: Significant reduction of surface solar irradiance induced by aerosols in a suburban region in northeastern China, *J. Geophys. Res.-Atmos.*, 112, D22S02, <https://doi.org/10.1029/2006JD007562>, 2007.
- Xiang B., Zhonglei X., Jing L., Linyan W., Xiqiang W., Mingwei C., Hui R.: Global PM<sub>2.5</sub>-attributable health burden from 1990 to 2017: Estimates from the Global Burden of disease study 2017, *Environmental Research*, 197, 111123, <https://doi.org/10.1016/j.envres.2021.111123>, 2021.
- Yu, W., Xu, R., Tingting, Y., Abramson, M. J., Morawska, L., Jalaludin. B., Johnston. F. H., Henderson, S. B., Knibbs, L. D., Morgan, G. G., Lavigne, E., Heyworth, J., Hales. S., Marks, G. B., Woodward, A., Michelle, L. B., Samet, J. M., Song, J., Li,



- 1060 S., Guo, Y.: Estimates of global mortality burden associated with short-term exposure to fine particulate matter (PM<sub>2.5</sub>), *The Lancet Planetary Health*, 8.3: e146-e155, 10.1016/S2542-5196(24)00003-2, 2024.
- Yamamoto, G. and Tanaka, M.: Determination of Aerosol Size Distribution from Spectral Attenuation Measurements, *Appl. Opt.*, 8, 447–453, <https://doi.org/10.1364/AO.8.000447>, 1969.
- Zhang D., Li Z., Wu H., Wu T., Ren R., Cai Z., Liang C., Chen L., Analysis of aerosol particle number size distribution and  
1065 source attribution at three megacities in China, *Atmospheric Environment*, 279, 119114, 1352-2310, <https://doi.org/10.1016/j.atmosenv.2022.119114>, 2022.
- Zhang, X., Li, L., Che, H., Dubovik, O., Derimian, Y., Holben, B., Gupta, P., Eck, T. F., Lind, E. S., Toledano, C., Xia, X.,  
Zheng, Y., Gui, K., and Zhang, X.: Aerosol Components Derived from Global AERONET Measurements by GRASP: A New  
Value-Added Aerosol Component Global Dataset and Its Application, *B. Am. Meteor. Soc.*, 105, E1822–E1848,  
1070 <https://doi.org/10.1175/BAMS-D-23-0260.1>, 2024.
- Zuber, R., Sperfeld, P., Riechelmann, S., Nevas, S., Sildoja, M., and Seckmeyer, G.: Adaption of an array spectroradiometer  
for total ozone column retrieval using direct solar irradiance measurements in the UV spectral range, *Atmos. Meas. Tech.*, 11,  
2477–2484, <https://doi.org/10.5194/amt-11-2477-2018>, 2018.
- Zuber, R., Köhler, U., Egli, L., Ribnitzky, M., Steinbrecht, W., and Gröbner, J.: Total ozone column intercomparison of  
1075 Brewers, Dobsons, and BTS-Solar at Hohenpeißenberg and Davos in 2019/2020, *Atmos. Meas. Tech.*, 14, 4915–4928,  
<https://doi.org/10.5194/amt-14-4915-2021>, 2021.

## Appendix

Table A1: List of abbreviations.

GAW-PFR	Global Atmospheric Watch-Precision Filter Radiometer
AERONET	Aerosol Robotic Network
WMO	World Meteorological Organization
GRASP	Generalized Retrieval of Atmosphere and Surface Properties
PFR	Precision Filter Radiometer



---

CIMEL	CIMEL CE318-TS sun and sky photometer
BTS	The array spectroradiometer 'BiTec Sensor'.
POM	PREDE-POM sun and sky radiometer
FRC	Filter Radiometer Comparison
AOD	Aerosol Optical Depth
AE	Angström Exponent
DSI	Direct Solar Irradiance
AOD <sub>f</sub>	Fine Mode Aerosol Optical Depth
AOD <sub>c</sub>	Coarse Mode Aerosol Optical Depth
C <sub>VT</sub>	Total Volume Concentration
C <sub>Vf</sub>	Fine Mode Volume Concentration
C <sub>Vc</sub>	Coarse Mode Volume Concentration
R <sub>eff</sub>	Effective Radius
R <sub>Vf</sub>	Fine Mode Volume Median Radius
R <sub>Vc</sub>	Coarse Mode Volume Median Radius

---



---

$\sigma_{vf}$	Fine Mode Geometric Standard Deviation
$\sigma_{vc}$	Coarse Mode Geometric Standard Deviation
FMF	Fine mode fraction of AOD
RRI	Real part of the aerosol Refractive Index
IRI	Imaginary part of the aerosol Refractive Index
SSA	Single Scattering Albedo
SD	Aerosol Size Distribution
GRASP-PFR	Aerosol Properties Retrieval(s) using the AOD observed by a PFR as input.
GRASP-BTS	Aerosol Properties Retrieval(s) using the AOD observed by a BTS as input.
AER-SKY	AERONET retrievals of aerosol properties using the sky radiance measured in the almucantar geometry.
AER-SDA	AERONET retrievals of aerosol optical depth modal separation using the spectral deconvolution algorithm.
SZA	Solar zenith angle
FoV	Field-of-View Angle
FWHM	Full-Width-at-Half-Maximum
St.d.	Standard Deviation

---



---

R	Pearson correlation factor
R <sup>2</sup>	Coefficient of determination
RMSE	Root mean square error
AOD-obs	AOD retrieved directly from the direct spectral irradiance measured by an instrument.
AOD-ext	AOD estimated by the Angström law after calculation of the Angström exponent and turbidity coefficient using observed spectral AOD.
UV	Ultraviolet
IR	Infrared
O <sub>3</sub>	Ozone
H <sub>2</sub> O	Water vapour
CH <sub>4</sub>	Methane
N <sub>2</sub> O	Nitrous oxide